Journal of Neuroinflammation

RESEARCH

Open Access

Inhibition of neutrophil extracellular traps alleviates blood–brain barrier disruption and cognitive dysfunction via Wnt3/β-catenin/TCF4 signaling in sepsis-associated encephalopathy

Jianhe Yue[1,2†], Lijuan Mo[3†], Guotao Zeng[2†], Ping Ma[2], Xiaolin Zhang[2], Yuhang Peng[2], Xiang Zhang[2], You Zhou[4], Yongxiang Jiang[2], Ning Huang[2*] and Yuan Cheng[2*]

Abstract

Background Neutrophils and neutrophil extracellular traps (NETs) have been identified as crucial contributors in several neuroinflammatory models, such as stroke and traumatic brain injury, but their role in sepsis-associated encephalopathy (SAE) has not been thoroughly investigated.

Methods In this study, we established an SAE model using cecal ligation puncture (CLP) surgery to examine neutrophil infiltration and NETs formation. A protein arginine deiminase 4 (PAD4) inhibitor, GSK484, was employed to suppress NETs release. To assess changes in hippocampal gene expression induced by GSK484 treatment in CLP mice, we utilized RNA sequencing (RNA-Seq) combined with bioinformatics analysis. Additionally, the Elisa, cognitive function test, western bolt and immunofluorescence staining were used to measured hippocampal inflammatory cytokine, cognitive function, and the protein levels of tight junctions (TJs) and adherens junctions (AJs) in SAE mice. We also established a Transwell™ co-culture system using bEnd.3 cells and bone marrow-derived neutrophils to examine the effects of GSK484 on endothelial cell function. This comprehensive approach allowed us to evaluate the impact of NETs inhibition on neuroinflammation, cognitive function, and the underlying molecular mechanisms in the CLP-induced SAE model.

Results Our findings revealed that neutrophils were significantly overactivated, releasing abundant NETs in the hippocampus of CLP-induced SAE mice. Inhibition of NET formation using GSK484 led to reduced neuroinflammatory responses, improved blood–brain barrier (BBB) integrity, and enhanced survival rates and cognitive function in SAE mice. RNA-Seq and bioinformatics analyses identified the Wnt signaling pathway as the most significant pathway affected. Subsequent experiments demonstrated that NETs inhibition alleviated BBB damage primarily by increasing

†Jianhe Yue, Lijuan Mo and Guotao Zeng are co-first authors and contributed equally to this work.

*Correspondence:
Ning Huang
304237@hospital.cqmu.edu.cn
Yuan Cheng
Chengyuan@hospital.cqmu.edu.cn
Full list of author information is available at the end of the article

the expression of Occludin, a TJs protein, and promoting the formation of the VCL/β-catenin/VE-cadherin complex at AJs, mediated by the Wnt3/β-catenin/TCF4 signaling pathway.

Conclusions Our results suggest that inhibition of NETs may protect BBB permeability and cognitive function through the Wnt3/β-catenin/TCF4 signaling pathway in the context of CLP-induced SAE, which provides a promising strategy for SAE therapy.

Keywords Neutrophil extracellular traps, Sepsis-associated encephalopathy, Neuroinflammation, Blood–brain barrier, Adhesion junction

Introduction

Sepsis is defined as a life-threatening organ dysfunction resulting from a dysregulated host's reaction to infection. It affects a shockingly high number of patients, with estimates ranging from 19 to 48.9 million cases per year worldwide, making it a leading cause of death globally [1]. Despite significant clinical and therapeutic efforts, mortality rates remain high, with approximately 11.0 million sepsis-related deaths reported, accounting for 19.7% of all global deaths [2]. Sepsis dramatically impacts multiple organs, including the liver, kidneys, lungs, gut, and brain [3]. As one of the organs affected by sepsis, approximately 9% to 71% of patients with severe sepsis may develop sepsis-associated encephalopathy (SAE) [4]. SAE is responsible for short-term morbidity, prolonged hospital stay, long-term physical and cognitive impairment, and poses a large economic burden to healthcare systems [5]. The primary pathogenesis of SAE is driven by endotoxemia, which triggers the systemic release of pro-inflammatory cytokines. These cytokines activate immune cells, leading to a cycle of inflammation that exacerbates brain dysfunction and contributes to the progression of SAE [6]. Nevertheless, the specific molecular mechanisms underlying this neuroinflammatory response remain unclear.

Neutrophils are essential components of the innate immune system and serve as the first line of defense against infectious agents [7]. Following blood–brain barrier (BBB) injury, neutrophils are among the first peripheral immune cells recruited to the brain [8]. They primarily contribute to the inflammatory response through phagocytosis and the secretion of inflammatory mediators [9, 10]. Additionally, activated neutrophils release web-like structures known as neutrophil extracellular traps (NETs), which consist of tangled decondensed DNA, histones, myeloperoxidase (MPO), and other granular components [11, 12]. NETs are a double-edged sword, serving as both an essential initial line of defense against invading pathogens and, in certain cases, excessive NETs release may induce endothelial cells (ECs) to shift toward a pro-inflammatory phenotype [10, 12]. An increasing number of studies have shown that NETs mediate brain damage under various neuroinflammatory conditions, including trauma, stroke, and neurodegenerative diseases [9, 13–15]. Nevertheless, the specific role of NETs in SAE has yet to be comprehensively investigated.

In sepsis, pathogen-associated molecular patterns (PAMPs) and damage-associated molecular patterns (DAMPs) activate neutrophils, which combat infections through three primary mechanisms: phagocytosis, degranulation, and the release of NETs[16]. NETs, composed of histones, MPO, elastase, and other proteases [12], directly result in endothelial permeability, endothelial barrier dysfunction, and the disruption of adherens junctions (AJs) and actin cytoskeleton reorganization [12, 17]. In vitro studies suggest that NETs can promote endothelial dysfunction, as indicated by increased endothelial expression of ICAM-1, VCAM-1, E-selectin, tissue factor, and von Willebrand factor [17]. These mediators play a crucial role in endothelial dysfunction, including damage to cerebrovascular ECs. Cerebrovascular EC injury and BBB leakage have been observed as early as 6–8 h after the onset of sepsis [18]. Alongside BBB damage, the infiltration of neutrophils, NETs, and pro-inflammatory cytokines into the brain [19], triggers microglial and astrocyte activation, leading to the release of large quantities of inflammatory factors [20]. This cascade further exacerbates endothelial injury and BBB disruption. In SAE mice. Zhu et al. reported that NETs were found to be abundant in both the blood and hippocampus of CLP mice, and the degradation of NETs with DNase I alleviated sepsis-induced changes in the hippocampus, suggesting a key role for NETs in the development of this disease [11]. However, while these findings are promising, the molecular mechanisms underlying the neuroprotective effects of NET inhibition in SAE remain largely unexplored and require further investigation.

Protein arginine deiminase (PAD) enzymes are widely distributed in mammals and are closely related to cell development and differentiation [21]. PADs convert protein Arg residues into citrulline in a calcium and sulfhydryl-dependent manner, which plays a key role in physiological and pathological processes [22]. There are five types of PAD enzymes in human and mouse, including PAD4 [23]. PAD4 catalyzes citrullination of histones and promotes chromatin decondensation [23]. GSK484,

a potent and selective antagonist of PAD4, could effectively inhibit the formation of NETs in the brain and blood effectively [24]. Previous studies demonstrated that GSK484 administration significantly reduced brain edema and neuronal injury following subarachnoid hemorrhage [24]. Additionally, in models of traumatic brain injury (TBI) and cerebral ischemia–reperfusion injury (CIRI), GSK484 effectively attenuated neuroinflammation, improved neurological deficits, and enhanced survival rates [25].

Here, we demonstrated that the inhibition of NETs formation using GSK484, enhances the integrity of the BBB by promoting the expression of TJs proteins and facilitating the formation of the VCL/β-catenin/VE-cadherin complex. This inhibition also alleviates cognitive dysfunction and neuroinflammatory responses, primarily through the activation of the Wnt3/β-catenin/TCF4 signaling pathway. Conversely, the use of LF3, an antagonist of β-catenin/TCF4, counteracted the protective effects of GSK484, leading to disruption of both tight junctions (TJs) and AJs. Collectively, these findings showed that inhibiting NET formation plays a crucial role in improving BBB function and mitigating cognitive dysfunction and neuroinflammatory responses via the Wnt3/β-catenin/TCF4 signaling pathway.

Materials and methods

All antibodies, reagents, vendors, catalogue numbers, and concentrations or dilution ratios are shown in detail in Suppl. Table 1.

Animals

Male C57BL/6 mice (8–10 weeks old and 22–25 g) were purchased from the Byrness Weil biotechnology Ltd (Chongqing, China). Prior to the experiments, the mice were acclimated for at least one week in an environment with controlled humidity (55–65%) and temperature (20–23 °C), under a 12-h light/dark cycle. The animal program was authorized by the Institutional Animal Care and Use Committee of Chongqing Medical University Affiliated Second Hospital (Chongqing, China).

Cecal ligation and puncture (CLP) model

SAE was established by CLP as previously described [26–28]. Briefly, mice were anesthetized with isoflurane, and a 2 cm-wide midline laparotomy was performed to expose the cecum. The cecum was ligated with a 4.0 silk suture at 1/4 distance to the end below the ileocecal flap and then punctured with a 22G sterilized needle. Intestinal contents were pushed out through the perforation site. The cecum was then returned to the peritoneal cavity, and the laparotomy was closed with 4.0 silk sutures. All animals received a dose of antibiotic (primaxin, 0.5 mg/mouse in 200 μL of sterile saline) subcutaneously immediately at the end of surgery. The animals were housed individually post-surgery with unrestricted access to food and water. In the sham group, mice underwent the same surgical procedures but without cecal ligation or puncture.

Intracerebroventricular cannulation and drug administration

Following anesthetization, mice were placed in the stereotaxic apparatus (RWD life science Co. Ltd., China). Following established protocols [29], guide cannulas (RWD life science Co. Ltd., China) were planted into the right lateral ventricle at coordinates 0.6 mm posterior to the bregma, 1.5 mm lateral, and 2 mm deep from the dura. The cannulas were secured with dental cement, and mice were allowed to recover in individual cages for 7 days. Daily handling was conducted to monitor cannula positioning and to habituate the animals to the investigators.

To investigate the role of NETs inhibition on SAE, we first set up three groups, namely, Sham, CLP, CLP + GSK484, and CLP + GSK484 group mice were administered 4 mg/kg (dissolved in sterile saline) of GSK484 (GLPBIO, USA), a PAD4 inhibitor, via tail vein injection. GSK484 was administered three days prior to and two days after CLP surgery [30], For β-catenin/TCF4 inhibition, LF3 (MCE, USA), a selective antagonist, was dissolved in a vehicle solution of 2% DMSO, 40% PEG300, 5% Tween-80, and 53% saline to achieve a final concentration of 250 mg/mL. We set up six groups, namely, Sham, CLP, Sham + GSK484, CLP + GSK484, CLP + GSK484 + Vehicle, CLP + GSK484 + LF3. The Vehicle and LF3 (5 μL) were administered intracerebroventricularly (i.c.v.) 30 min before CLP surgery and every 24 h thereafter.

Immunofluorescence (IF) staining

For IF analysis, paraffin embedding (4 μm) or frozen (12 μm) brain sections were incubated overnight at 4 °C with primary antibodies: ZO-1, Occludin, MSN, Fermt1, VCL, CD31, NeuN, GFAP, Iba1, MPO, Cit-H3, Ly6G, CD11b, β-catenin and VE-cadherin (details provided in Suppl. Table 1), in blocking solution. Following this, sections were treated with goat anti-mouse Alexa Fluor Plus 488/594/647 secondary antibodies (Invitrogen, USA) and subsequently mounted with a medium containing DAPI (Solarbio, China) in a dark environment. A multiplex immunofluorescence kit was also utilized as needed (AiFang biological, China). Images were captured under a fluorescent microscope (Olympus, Japan). Optical density was calibrated, and areas along with integrated densities were measured using ImageJ (USA). Changes in immunofluorescent intensity were calculated

as mean fluorescence intensity (integrated densities/areas).

Cell culture, neutrophil extraction, and construction of co-culture system

bEnd.3 cell lines were purchased from the Chinese Academy of Sciences Shanghai Cell Bank (Shanghai, China). The cells were cultured in Dulbecco's modified Eagle's essential medium (Gibco, USA) containing 10% fetal bovine serum (Gibco, USA) and 1% penicillin/streptomycin (Beyotime, China) under 37℃ and 5% CO2.

According to the manufacturer's instructions, bone marrow-derived neutrophils were isolated from mice using a neutrophil extraction kit (HISTOPAQUE-1119, HISTOPAQUE-1077, Sigma, USA). After extraction, the cells were resuspended in complete culture medium (RPMI-1640 + 10% FBS). The cells were cultured in a 37 °C incubator with 5% CO_2. On the following day, phorbol 12-myristate 13-acetate (PMA, 100 nM, Beyotime, China) was added to induce NETs formation for 12 h.

For co-culture *experiment 1*, neutrophils (1×10^5 cells) were seeded in the upper chamber of a 12-well Transwell™ plate, and bEnd.3 cells (1×10^5 cells) were cultured in the lower chamber. Four groups were established as follows: *Ctrl*: No treatment applied. *Co-culture + GSK484*: Neutrophils and bEnd.3 cells co-cultured with only GSK484 treatment. *Co-culture + PMA*: Neutrophils and bEnd.3 cells co-cultured with only PMA treatment. *Co-culture + PMA + GSK484*: Neutrophils and bEnd.3 cells co-cultured with PMA and GSK484 treatment.

For co-culture *experiment 2*, neutrophils (1×10^5 cells) were seeded in the upper chamber of a 12-well Transwell™ plate, and bEnd.3 cells (1×10^5 cells) were cultured in the lower chamber. Six groups were established as follows: *Ctrl*: No treatment applied. *Co-culture*: Neutrophils and bEnd.3 cells co-cultured without treatment. *Co-culture + PMA + Wnt3*: Neutrophils and bEnd.3 cells co-cultured with PMA and Wnt3 treatment. *Co-culture + PMA*: Neutrophils and bEnd.3 cells co-cultured with PMA treatment. *Co-culture + PMA + Wnt3 + GSK484*: Neutrophils and bEnd.3 cells co-cultured with PMA, Wnt3, and GSK484 treatment. *Co-culture + PMA + GSK484*: Neutrophils and bEnd.3 cells co-cultured with PMA and GSK484 treatment.

NETs staining in vivo and in vitro

NETs staining was performed as described in a previous study [31]. For in vivo staining, tissues were fixed with 4% paraformaldehyde, embedded in paraffin, and sectioned at 4 μm thickness. In vitro, neutrophils induced for NETs formation were fixed with 4% paraformaldehyde and permeabilized with 0.3% Triton X-100. In both in vivo and in vitro conditions, the primary antibody was incubated overnight at 4 °C. NETs were co-stained withMPO (1:50, Santa Cruz, USA), Citrullinated histone H3 (Cit-H3) (1:50, Abcam, UK), and DAPI (Solarbio, China). Positive NETs were identified by the presence of triple-positive (Cit-H3/MPO/DAPI) zone observed in multiple fields of view. Fluorescence images were captured using a fluorescence microscope (Olympus, Japan).

Brain water content (BWC)

The mice were euthanized at 72 h after surgery. The whole brain was instantly collected and weighed as the wet weight, and then dried at 100℃ for 24 h to acquire the dry weight. The BWC was calculated using the formula: $BWC = [(\text{wet weight} - \text{dry weight})/(\text{wet weight})] * 100\%$.

Fluorescein sodium (FS) permeability assay

FS was applied to evaluate BBB permeability as previously described [32]. Briefly, 2% FS (Sigma, USA) was injected through the femoral vein at 4 mL/kg under anesthesia at 71 h after modelling. After 1 h, all animals were euthanized and transcardially perfused with 0.9% saline for 20 min to remove the intravascular dye. The hippocampus was then dissected from the brain, weighed separately, homogenized in 0.5 mL of 60% trichloroacetic acid and incubated at 4 °C for 30 min. After centrifugation (12,000 rpm, 15 min), the FS concentration in the supernatant was measured at OD 440 nm by a microplate reader (BioTek, USA). We visualized FS leakage under a Fluorescence Scanning Microscope (KFBIO, China) using 12 μm frozen brain sections.

Morris water maze (MWM) test

Learning and memory were examined using a standardized 7-day MWM test, as described previously [33]. The MWM was conducted in a circular pool with a diameter of 125 cm and a height of 40 cm, filled with water to a depth of approximately 30 cm, maintaining a temperature of 20 ± 2 °C. A submerged platform with a diameter of 10 cm and a height of 29 cm was placed in the pool. Each mouse underwent six daily trials with a 1-min intertrial interval to locate the platform, being individually placed in one of four quadrants (the target quadrant where the platform was positioned). Each daily acquisition session included four trials per quadrant. A trial concluded once the mouse reached the platform or after 60 s had elapsed. If the mouse failed to find the platform within this time, it was gently guided to the platform and allowed to remain there for 10 s. After each session, the mice were carefully dried with a clean towel and returned to their home cage. On the final day, the platform was removed to conduct a probe trial, during which the number of crossings over

the target quadrant and the total time spent in the target quadrant were recorded (MED Associates, USA).

Open field test (OFT)

The locomotor and exploratory activities of mice were measured in an open-field apparatus. A mouse was gently placed in the center of a plastic chamber (50 × 50 × 40 cm) for 5 min, and its activities were automatically recorded using a video tracking system (MED Associates, USA). The total distance travelled and time spent in the center of the arena were recorded to assess the locomotor activity and spatial exploration of the mice. The apparatus was cleaned with 75% alcohol between tests to remove any odor cues.

Western blot (WB)

Proteins were extracted from hippocampus tissues or bEnd.3 cells in a lysis buffer (Solarbio, China) containing a protease inhibitor cocktail (Solarbio, China) and boiled in a SDS sample buffer (Beyotime, China) for 15 min. Nuclear proteins were extracted from homogenized tissues or cells using nuclear protein extraction kits (Solarbio, China), respectively. Equal amounts of protein per sample were separated by SDS-PAGE (8% or 10%) and electrotransferred to a polyvinylidene difluoride membrane (Milipore, USA). Membranes were blocked with 5% BSA (Beyotime, China) for 1 h at room temperature, and rinsed three times (10 min/time) with 0.5% PBST (0.5 mL Tween-20 in 1 L 0.01 M PBS). Next, incubated with the specified primary antibodies at 4℃ overnight, rinsed three times (10 min/time) with 0.5% PBST, and then 1 h with HRP-conjugated goat anti-rabbit IgG (detailed antibodies were shown in Suppl. Table 1), rinsed three times (10 min/time) with 0.5% PBST, followed by detection using an enhanced chemiluminescence kit (Milipore, USA). All uncropped Western blot image with markers were shown in Suppl. File 1.

Transcriptome sequencing

Mice were treated with saline or GSK484 (4 mg/kg) for 5 days (3 days before CLP and 2 days after CLP; n = 3). Total RNA was isolated using TRIzol (Invitrogen, USA), and genomic DNA was removed using DNase I (Takara, Japan). Subsequent steps included RNA purification, reverse transcription, library construction, and sequencing. The mRNA was fragmented, and the resulting short sequence fragments were sequenced using the BGI platform. The final library was sequenced on the DNBSEQ-T7 sequencer (MGI Tech Co., Ltd., China) using the PE150 model. The raw sequencing data were initially filtered with Trimmomatic (version 0.36). Clean data were aligned to the reference genome using STAR software (version 2.5.3a). Reads mapped to the exon regions of each gene were quantified using featureCounts (Subread-1.5.1; Bioconductor), followed by the calculation of RPKM values. Differential expression analysis was performed with the edgeR package (version 3.12.1), considering genes with a $p \leq 0.05$ as significantly differentially expressed genes (DEGs). Gene Ontology (GO) and Kyoto Encyclopedia of Genes and Genomes (KEGG) pathway enrichment analyses were conducted using R. The DEGs were uploaded to STRING (version 11.0), with a median confidence score of 0.2 to construct protein–protein interaction (PPI) networks. Cytoscape (v.3.7.2) was employed for PPI network visualization, while the CytoHubba plug-in was used to identify key modulators based on network metrics. Hub genes were predicted by screening important nodes within the PPI network modules, with the top 10 genes determined using the MCC, DMNC, MNC, Degree, and EPC algorithms. Additionally, the MCODE plug-in was utilized with default criteria to identify the top modules ranked by MCODE scores in descending order.

Cytokine examination

Expression levels of TNF-α, IL-6, IL-1β and IL-10 were quantified using a commercial ELISA kit (Boster Biological Technology, China). All procedures were carried out following the manufacturer's instructions.

Statistical analysis

Statistical analyses were performed with GraphPad Prism 9. All data were presented as mean ± SD and tested for normal distribution by Shapiro–Wilk test. For normally distributed data, differences between the two groups were compared by independent-sample t-tests. Meanwhile, differences among multiple means were assessed by one-way, two-way or repeated-measure of ANOVA, followed by a Bonferroni test whenever appropriate. The survival rate was analyzed by the Kaplan–Meier method and compared by the log-rank test. Statistical significance was set at $p < 0.05$.

Results

Dynamic expression of neutrophils and NETs after CLP over a period of time

With the aim of investigating the neuroinflammatory role of NETs formation, we conducted a series of experiments at various time points following sham or CLP operations, as detailed in Fig. 1A. Firstly, we designed a 7-day experiment to observe the time point of neutrophil accumulation after CLP. The IF co-staining of Ly-6G and CD11b revealed that the number of neutrophils began to increase at 8 h post-CLP, peaked at 48 h, and then returned to baseline levels by day 7 in the hippocampal CA1 region (Fig. 1B, C). Similarly, The IF co-staining

of Cit-H3/MPO/DAPI revealed that NETs started to increase at 12 h post-injury, peaked at 72 h, and then then gradually decrease in the hippocampal CA1 region (Fig. 1D, E). Based on these findings, we selected 72 h as the sacrifice time point for the CLP mice in subsequent experiments, unless otherwise specified. Having established the time course of neutrophil and NETs accumulation, we next sought to determine whether inhibiting NETs formation could mitigate neuroinflammation and cognitive impairments in SAE.

Pharmacological inhibition of NETs improved survival, reduced neuroinflammation, and alleviated cognitive impairment in SAE Mice

To investigate the specific role and underlying mechanism of NETs in the progression of SAE, we administered GSK484, a potent and reversible PAD4 inhibitor that blocks NETs formation, via intravenous injection 3 days before and 2 days after CLP surgery. We first investigated the effects of different drug doses on the mortality rate of CLP mice. Our results showed that higher doses of the drug did not further improve the survival rate of the CLP mice. Instead, when the dose reached 16 mg/kg, the mortality rate significantly increased compared to the 4 mg/kg dose group. A treatment dose of 8 mg/kg also appeared to increase the mortality rate, although the difference was not statistically significant. Based on literature reports [11], we selected 4 mg/kg as the therapeutic dose for further studies. (Fig. 2A). Treatment with 4 mg/kg of GSK484 significantly improved the body weight of the mice (Fig. 2B). As shown by Cit-H3/MPO/DAPI IF staining, the GSK484 treatment significantly reduced NETs formation in the hippocampus CA1 region (Fig. 2C, quantified in Fig. 2D). Moreover, GSK484 treatment diminished the production of key inflammatory cytokines (IL-6, IL-1β, TNF-α and IL-10) in the hippocampus of CLP mice (Fig. 2E–H), indicating a significant decrease in neuroinflammation. And treatment with GSK484 alone had no significant effect on the levels of inflammatory cytokines in the brain of the control group. To assess cognitive function, we conducted the MWM and OFT. The results showed that GSK484-treated mice exhibited significantly increased movement distance and time spent in the center in the OFT (Fig. 2I–K), and demonstrated improved performance in the MWM test (Fig. 2L–N), suggesting that NETs inhibition mitigated CLP-induced cognitive impairment. These results revealed that inhibiting NETs formation not only reduces neuroinflammation but also restores cognitive function, suggesting a critical role of NETs in both inflammatory and cognitive outcomes in SAE.

Inhibition of NETs formation via GSK484 induced global changes of septic mice in the hippocampus transcriptome

The RNA-Seq technique in combination with bioinformatics analysis was used to characterize alteration in the hippocampus gene expression after GSK484 treatment in CLP mice (All sequenced genes and their relative expression levels are shown Suppl. File. 2). Differentially expressed genes (DEGs) were identified using the DESeq2 R package, with 705 DEGs showing significant expression differences ($p < 0.05$) between the CLP and CLP + GSK484-treated groups. As depicted in Fig. 3A, the volcano plot illustrates 162 and 543 genes, which were significantly up- and down-regulated between two groups, respectively. To further analyze the biological significance of these DEGs, GO enrichment analysis was performed using the "clusterProfiler" R package, covering three categories: biological process (BP), cellular component (CC), and molecular function (MF). The top 10 terms for each category are displayed in a bar chart. Notably, DEGs were significantly enriched in "muscle organ development," "ERK1 and ERK2 cascade," and "negative regulation of protein phosphorylation" within the BP category. For the CC category, terms such as "collagen-containing extracellular matrix (ECM)," "main axon," and "adherens junction" were enriched, while in the MF category, "ECM structural constituent," "hormone binding," and "actin binding" were prominent (Fig. 3B). These results uncovered that GSK484 treatment predominantly affected genes related to inflammation, cell adhesion, and cellular structure. Functional annotation and KEGG pathway analysis were also conducted on the DEGs using R software. The top 10 enriched pathways included "cytoskeleton in muscle cells," "gastric acid secretion," "Wnt signaling pathway," "hepatocellular

(See figure on next page.)

Fig. 1 Dynamic expression of neutrophils and NETs after CLP over a period of time. **A** Schematic timeline of the experimental procedures. **B** and **C** Representative photographs of IF co-staining of Ly-6G and CD11b, a neutrophil biomarker, and quantification of the number of Ly-6G/CD11b + cell in the hippocampal CA1 region of mice from the sham group and CLP group at 4 h, 8 h, 12 h, 24 h, 48 h, 72 h, 5 days and 7 days (n = 6). **D** and **E** Representative photographs of IF staining of Cit-H3 with MPO, a NETs biomarker, and quantification of the number of Cit-H3/MPO/DAPI + cells in the hippocampal CA1 region of mice from the sham group and CLP group at 4 h, 8 h, 12 h, 24 h, 48 h, 72 h, 5 days and 7 days (n = 6). Nuclei were stained with DAPI. Scale bar = 20 μm. NETs: Neutrophil extracellular traps, CLP: Cecal Ligation and Puncture; Cit-H3: Citrullinated histones H3; MPO: Myeloperoxidase; IF: immunofluorescence. (Data are expressed as the mean ± SD. *$p < 0.05$ compared with sham, ns: no significance, *$p < 0.05$, **$p < 0.01$, ***$p < 0.001$, ****$p < 0.0001$)

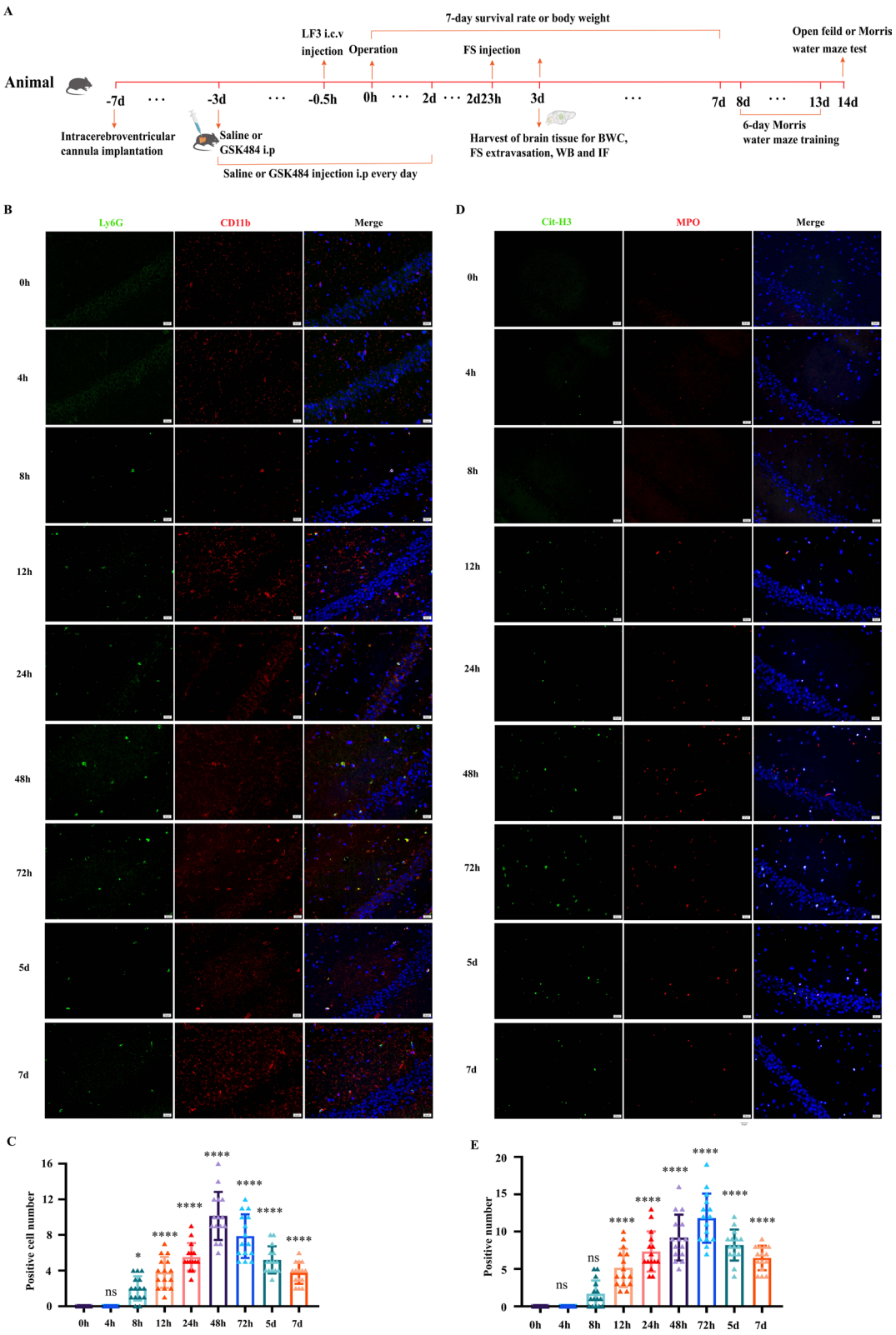

Fig. 1 (See legend on previous page.)

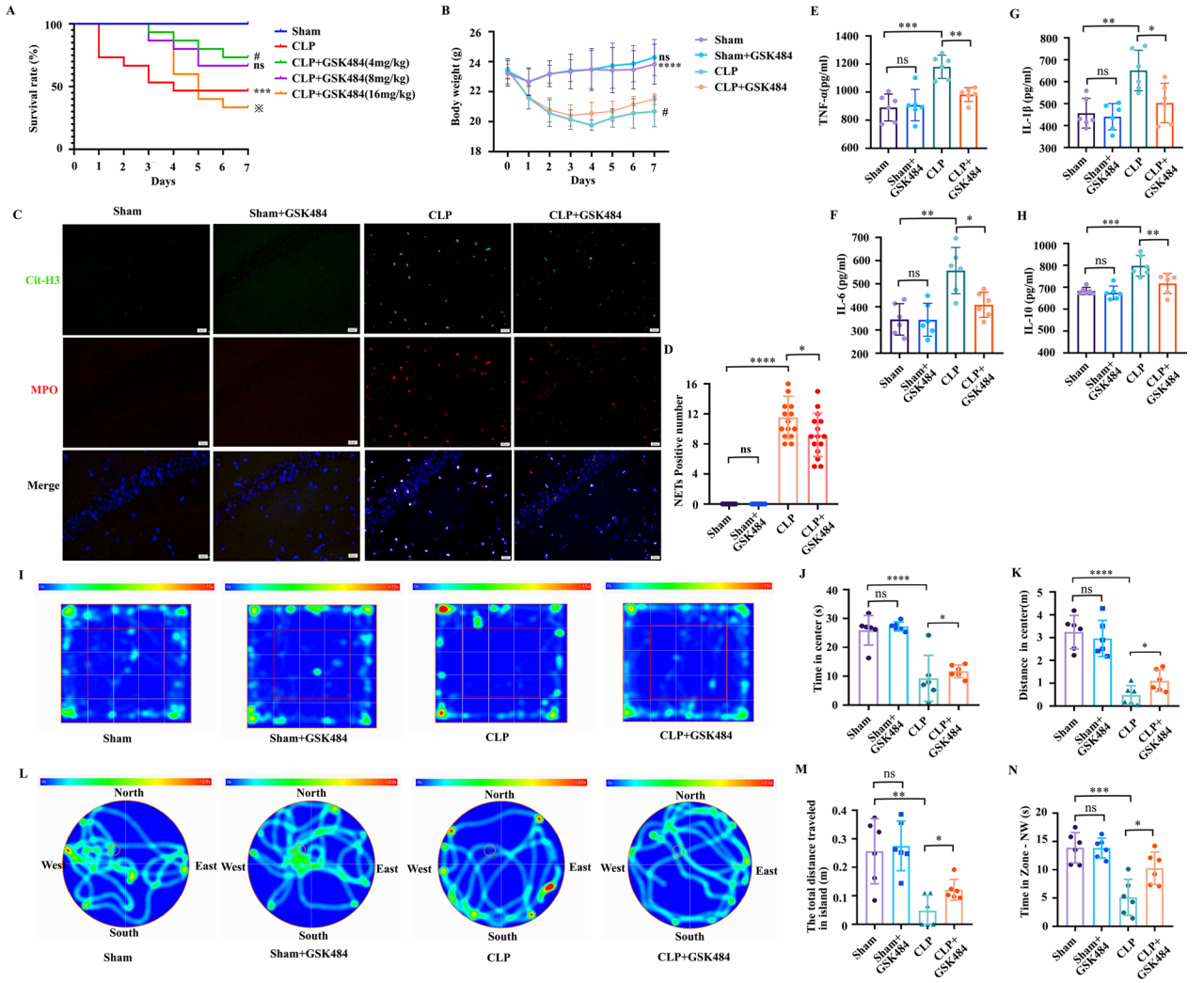

Fig. 2 The inhibition of NETs formation improved SAE mice survival, defended neuroinflammation and alleviated cognitive impairment. **A** 7-day survival rates of SAE mice treated with different concentrations of GSK484 (n = 15). **B** Quantification of NETs numbers (n = 6). **C** and **D** GSK484 inhibited NETs formation in the CA1 region of the hippocampus by IF staining (n = 6). **E**–**H** ELISA test showed that GSK484 decreased the levels of TNF-α, IL-6, IL-1β and IL-10 in hippocampus tissue (n = 6). **I** The trace heat map of OFT. The time (**J**) and the movement distance (**K**) in center in OFT. **L** The trace heat map of MWM test. The movement distance (**M**) in island, and the time (**N**) in NW area in the MWM test were increased after GSK484 treatment (n = 6). NETs: Neutrophil extracellular traps; CLP: Cecal Ligation and Puncture; SAE: Sepsis-associated encephalopathy; IF: immunofluorescence; OFT: open field test; MWM: Morris water maze. (ns: no significance, *$p < 0.05$, **$p < 0.01$, ***$p < 0.001$, ****$p < 0.0001$)

carcinoma," "proteoglycans in cancer," "breast cancer," "oxytocin signaling pathway," "mTOR signaling pathway," "Cushing syndrome," and "human papillomavirus infection" (Fig. 3C). Among these, the Wnt signaling pathway was the most significantly enriched, suggesting that it may play a key regulatory role in the protective effects observed after GSK484 treatment.

Next, the DEGs were uploaded to the STRING database for PPIs analysis, and visualized the PPI networks using Cytoscape software to identify key gene interactions (Fig. 3D). We applied five different algorithms to identify the top 10 hub genes based on the CytoHubba plug-in in Cytoscape (Fig. 3E), which included *VCL, Cldn11, MSN, Ocln, Fermt1, Gia1, Pik3r1, Xbp1, Mbp,* and *Esr1*. Notably, the top five hub genes primarily encoded proteins involved in AJs, TJs and cellular structural related proteins. Using the MCODE plugin, we identified two functional modules based on their MCODE scores. The top module, consisting of three genes—*VCL, MSN*, and *Fermt1*—was selected for further visualization (Fig. 3F). These data supposed that Wnt signaling pathway and downstream key genes related to AJs, TJs, and cellular structure were modulated after inhibition of NETs formation in CLP-induced SAE model.

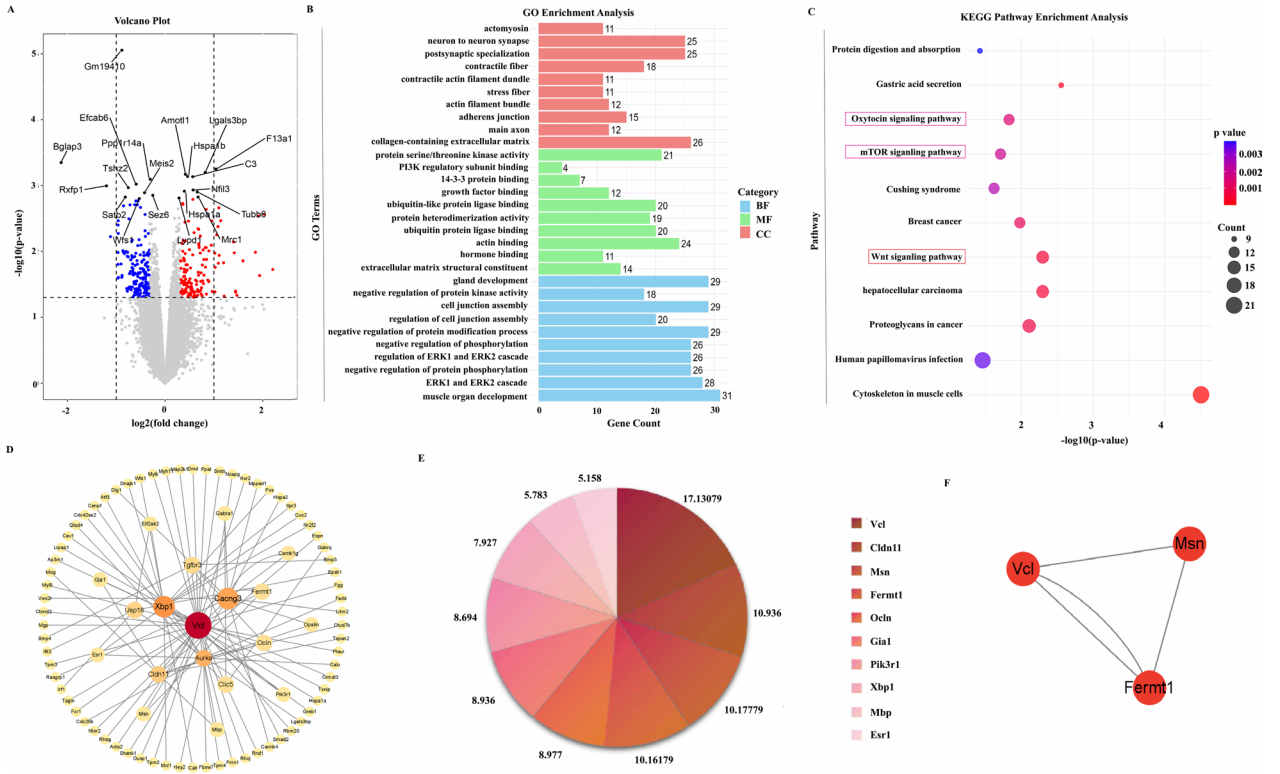

Fig. 3 Distinct transcriptional signature between CLP- and GSK484-treated hippocampus. **A** A vulcano plot was depicted with $p < 0.05$ of all 705 detected genes from RNA-Seq dataset. Differential expression genes (DEGs) were colored with blue and red, regarding to 163 down-regulated and 542 up-regulated genes, respectively. **B** Bar plot of GO enrichment analysis; (BP) biological process, (CC) cellular components, (MF) molecular function. **C** Bubble plot of KEGG pathway analysis. **D** Cytoscape was used to visualize the PPI network generated by String. **E** The top 10 hub genes were obtained using the CytoHubba plug-in in Cytoscape. **F** The top 1 modules are presented based on MCODE scores in descending order. DEGs: Differential expression genes; BP: biological process; CC: cellular components; MF: molecular function; CLP: Cecal Ligation and Puncture; GO: Gene Ontology; KEGG: Kyoto Encyclopedia of Genes and Genomes

The inhibition of NETs formation protected BBB integrity by alleviating TJs disruption in brain ECs

To assess brain damage, we first measured BWC. At 72 h post-CLP, BWC was significantly increased in CLP mice compared to sham controls. GSK484 treatment notably decreased BWC in the CLP group ($p < 0.05$, Fig. 4A). FS extravasation, a marker for BBB disruption, was used to further evaluate BBB integrity [28]. As shown in Fig. 4B, C, the FS levels in both the hippocampus and global brain tissues were markedly elevated in CLP mice but were significantly reduced following GSK484 administration, and representative sections for FS leakage are shown in Fig. 4D. And treatment with GSK484 alone had no significant effect on BWC or FS extravasation in the brain of the control group. These findings suggested that NETs contribute BBB leakage, and inhibiting NETs formation could effectively attenuate the BBB leakage in CLP-induced SAE mice.

Based on bioinformatics analysis, the top 5 hub genes have been identified through the CytoHubba plug-in in Cytoscape, including *VCL* (Vinculin, a cytoskeletal protein involved in cell–cell and cell–matrix junctions), *Cldn11* (Claudin-11, a component of TJs and CNS myelin), *MSN* (Moesin, which links the cell membrane to the cytoskeleton), *Ocln* (Occludin, a key TJ protein), and *Fermt1* (Fermt1, involved in integrin signaling and the connection of the actin cytoskeleton to the ECM, and a negative regulator of Wnt/β-catenin signaling). These hub genes primarily encode proteins associated with TJs, AJs, and cellular structure. Therefore, we first analyzed the expression of major TJs-related genes in the hippocampus from our RNA-seq data (mRNA expression is obtained from RNA-seq data shown in Suppl. File. 2).

The barrier function of BBB is primarily depends on brain ECs and their TJs proteins, those proteins seal contact sites between ECs, which seal contact sites between ECs and block the paracellular transport of ions, macromolecules, and polar solutes [34]. TJs are consist of integral membrane proteins such as Claudin, Occludin, along with cytoplasmic accessory proteins like Zonula occludens (ZO-1, ZO-2, ZO-3), and junction adhesion molecules (JAMs) and cingulin [35]. Furthermore, we

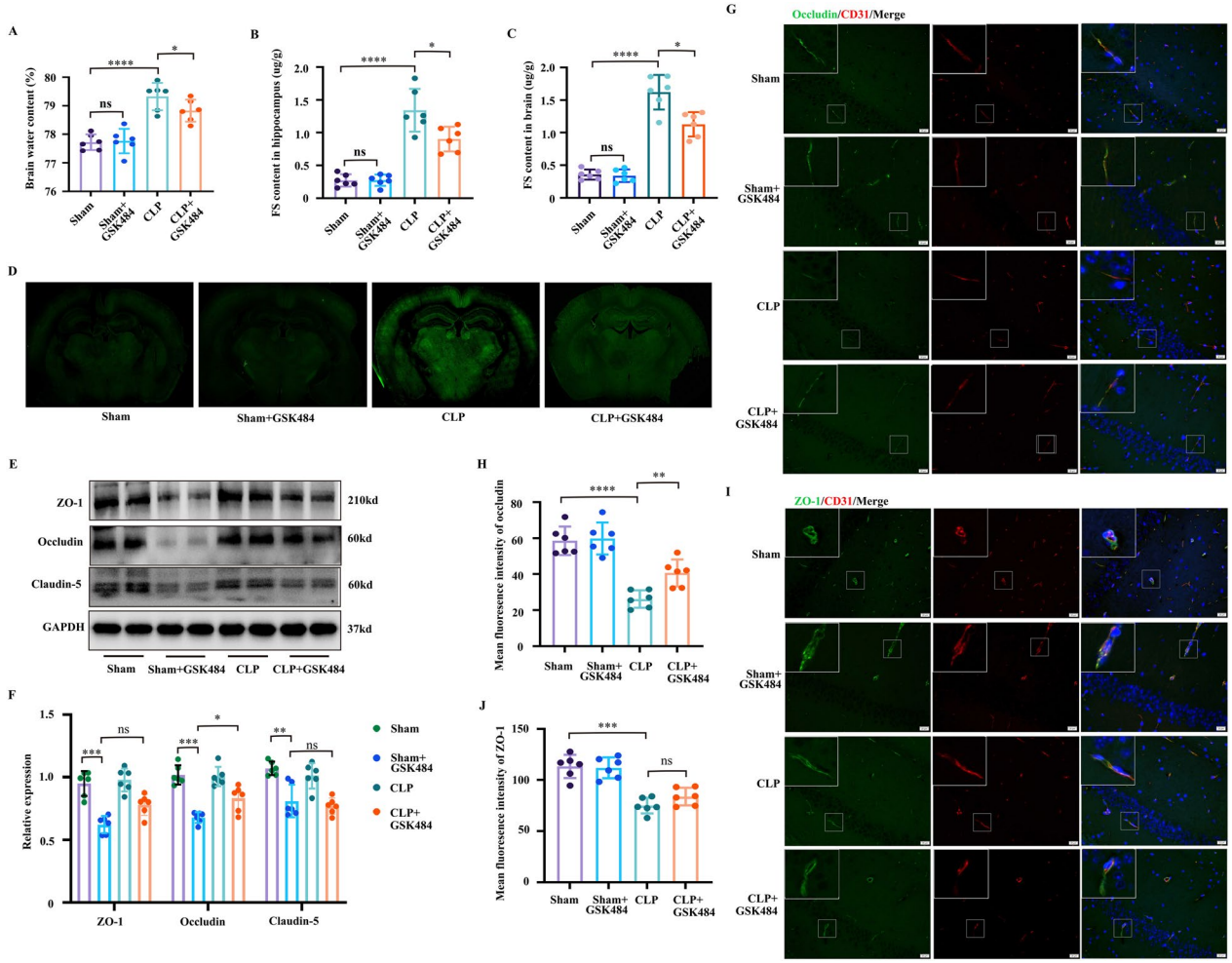

Fig. 4 The inhibition of NETs formation reduced BBB permeability in SAE mice by alleviating TJs disruption. **A** The BWC was measured. Quantification of the FS extravasation in the hippocampus (**B**) and the global brain tissue (**C**) (n = 6). **D** Representative images showing the extravasation of FS. **E** Expression levels of TJs (ZO-1, Occludin, Claudin-5) proteins in the hippocampus were detected by Western blot (n = 6). **F** Expression levels of TJ proteins were quantified and normalized to GAPDH levels (n = 6). Double labeling shows colocalization of Occludin (**G**) and ZO-1 (**I**) with ECs (CD31) in the CA1 region of the hippocampus (40x, n = 6). Quantification of the fluorescence intensity of Occludin (**H**) and ZO-1 (**J**) in the hippocampus. NETs: Neutrophil extracellular traps; CLP: Cecal Ligation and Puncture; SAE: Sepsis-associated encephalopathy; ECs: endothelial cells; BBB: Blood–brain barrier; TJs: Tight junctions; BWC: Brain water content; FS: Fluorescein sodium. (ns: no significance, *$p < 0.05$, **$p < 0.01$, ***$p < 0.001$, ****$p < 0.0001$)

evaluated major TJs proteins expression, including ZO-1, Claudin-5, and Occludin in the hippocampus using WB analysis. As shown in Fig. 4E, F, the protein expression levels of ZO-1, Occludin and Claudin-5 were sharply downregulated in the CLP group compared to the sham group ($p < 0.05$). GSK484 treatment specifically restored Occludin expression ($p < 0.05$) but had no significant effect on ZO-1 or Claudin-5 levels.

We also assessed the distribution of TJs between ECs in the hippocampus using double IF staining. CLP-induced neuroinflammation disrupted the distribution of ZO-1 and Occludin, spreading them in the form of a dotted appearance and weakening their fluorescence intensity (Fig. 4G–J), suggesting a loss of protein–protein interactions within the TJs. However, GSK484 treatment restored Occludin distribution, forming a continuous line with enhanced fluorescence intensity. In contrast, the distribution and intensity of ZO-1 showed only limited improvement. These data reveal that NETs play a critical role in maintaining TJs integrity, and their excessive activation leads to TJs disintegration and BBB disruption. Inhibiting NETs formation protects the BBB primarily by promoting Occludin expression in brain ECs.

Additionally, *Cldn11*, one of the top 5 hub genes, encodes Claudin-11, a critical component of central nervous system (CNS) myelin, rather than a major TJs protein. [36–38]. Our WB results showed that its protein expression level was sharply downregulated in the CLP group compared to the sham group ($p < 0.05$). GSK484 treatment failed to restore its expression, and further reduced its expression (Suppl. Figures 1A-1B). Furthermore, the IF results showed that Claudin-11 is predominantly expressed in neurons within the CA1 region of the hippocampus (Suppl. Figure 1C). Treatment with GSK484 led to a reduction in Claudin-11 expression in neuronal cell, which may suggest potential injury to neuronal fibers. To further investigate whether GSK484 exerts a protective effect on endothelial cells, we conducted a co-culture experiment with NE and bEnd.3 cells. Our findings revealed that treatment with GSK484 alone had little effect on the fluorescence intensity and continuity of Occludin expression in bEnd.3 cells. However, after NETs formation was induced with PMA, GSK484 treatment significantly enhanced the fluorescence intensity and continuity of Occludin expression (Suppl. Figures 1D-1E).

The inhibition of NETs formation alleviated BBB AJs disruption in SAE mice.

In addition to TJs that regulate the paracellular endothelial barrier properties, AJs also play a crucial role in cell–cell adhesion at the BBB [39]. AJs are composed of key proteins such as cadherins, actin, catenin, and vinculin (VCL), which have been identified in microvessels of the BBB [40]. Based on bioinformatics analysis, the remaining three genes (*VCL, MSN* and *Fermt1*) among the top 5 hub genes are all associated with AJs proteins. We then analyzed the expression of these three genes in the hippocampus from our RNA-seq data (mRNA expression is obtained from RNA-seq data shown in Suppl. File. 2). To further validate the findings, we assessed the expression of the corresponding proteins in the hippocampus using WB. As shown in Fig. 5A–D, the protein expression of VCL, VE-cadherin and Fermt1 were significantly reduced in the CLP group compared to the sham group ($p < 0.05$).

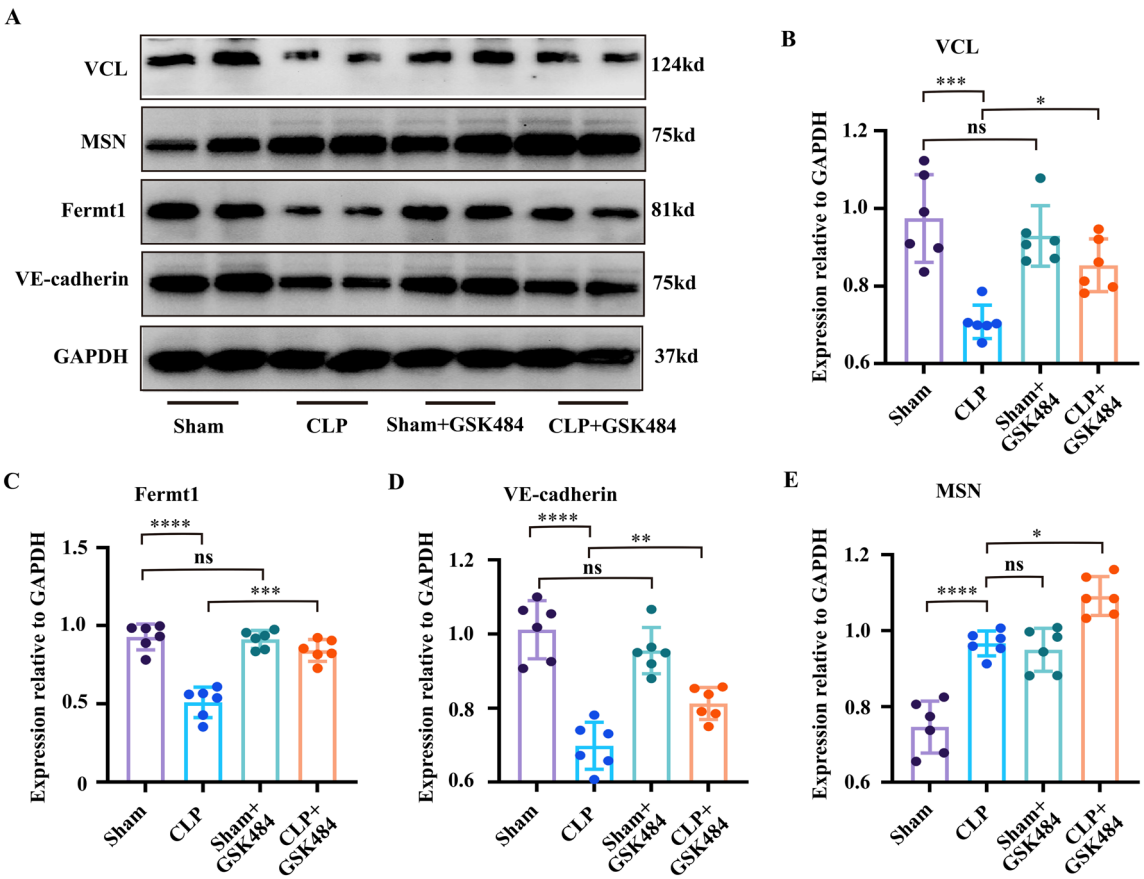

Fig. 5 The inhibition of NETs formation alleviated BBB AJs associated proteins in SAE mice. **A** Expression levels of AJs associated proteins in the hippocampus were detected by Western blot (n = 6). **B**–**E** The quantification analysis of AJs associated proteins expression levels (n = 6). (*$p < 0.05$, **$p < 0.01$, ***$p < 0.001$, ****$p < 0.0001$)

GSK484 treatment notably increased the expression of those proteins in CLP mice ($p < 0.05$). Interesting, MSN protein levels were significantly elevated in the CLP group ($p < 0.05$) and were further increased following GSK484 treatment ($p < 0.05$, Fig. 5E). These results suggest that the protective effects of inhibiting NETs formation are not limited to TJs but also involve AJs and the remodeling of cellular structure. The modulation of these proteins highlights the role of NETs in maintaining BBB integrity by regulating both junctional and cytoskeletal components.

Inhibiting NETs formation alleviated AJs damage by promoting VCL/β-catenin/VE-cadherin complex formation in SAE mice

Using the MCODE plugin, we identified a key module consisting of three genes: *VCL, Fermt1* and *MSN*. To explore the expression and distribution of these genes after GSK484 treatment, we performed double IF staining in the hippocampus. As shown in Fig. 6A, B, VCL was primarily expressed in brain ECs and not in microglia, astrocytes, or neurons. A similar distribution pattern was observed for Fermt1 (Fig. 6C, D). In contrast, MSN showed a broader expression, being present in both ECs and glial cells, including microglia and astrocytes (Suppl. Figures 2A-2B). These findings suggest that the top module genes are mainly involved in regulating the BBB in the CLP-induced SAE model.

Next, we assessed the protein expression levels and distribution of VCL, Fermt1 and MSN. Both VCL and Fermt1 protein are associated with cell adhesion, with VCL localizing to focal adhesion complexes [41] and Fermt1 linking the cellular actin cytoskeleton to the ECM via integrin signaling [42]. In the CLP group, fluorescence intensity for VCL (Fig. 7A–C) and Fermt1 (Fig. 7D–F) was significantly lower than in the sham group, but GSK484 treatment notably increased their expression levels in both CD31-positive and total areas ($p < 0.05$). This suggests that inhibiting NETs formation may reduce AJs disruption by increasing the levels of AJs proteins. MSN, a protein involved in linking the plasma membrane to the actin cytoskeleton, plays a crucial role in cellular morphology and motility [43]. IF staining revealed that the mean fluorescence intensity of MSN was higher in the CLP group compared to the sham group, and further increased after GSK484 treatment ($p < 0.05$, Suppl. Figures 3A-3B). While MSN levels in CD31-positive areas were also elevated in the CLP group, GSK484 treatment did not further enhance MSN expression in these areas (Suppl. Figure 3C). These findings suggested that MSN-mediated cellular status changes may not be closely related to cell adhesion of ECs.

The interaction between VCL and β-catenin is essential for stabilizing cadherins at the cell surface, which ensures that the junctions between ECs remain intact, thereby preventing the paracellular passage of substances [44]. VE-cadherin, an endothelial-specific adhesion protein, regulates EC permeability [45]. To investigate the interaction among VCL, β-catenin, and VE-cadherin, we performed triple labeling. Colocalization of VCL, β-catenin, and VE-cadherin (Fig. 8A) indicated their potential function as a complex. Quantification showed no significant difference in β-catenin expression in the total area among the sham, CLP, and CLP + GSK484 groups (Fig. 8C), consistent with WB data. However, VCL (Fig. 8B) and VE-cadherin (Fig. 8D) expression levels were reduced in CLP mice but were significantly increased following GSK484 treatment ($p < 0.05$). In summary, inhibition of NETs formation alleviates AJs disruption, likely by promoting the formation of the VCL/β-catenin/VE-cadherin complex, thereby preserving EC adhesion barrier and BBB integrity in SAE mice. The close interaction between VCL, β-catenin, and VE-cadherin is particularly relevant for BBB integrity, as it ensures that the junctions between ECs remain intact, preventing the paracellular passage of substances that could compromise brain homeostasis.

Inhibition of NETs by GSK484 enhances BBB integrity via Wnt3/β-Catenin/TCF4 signaling: in vitro and in vivo insights

Through RNA-seq and bioinformatics analysis, we identified the Wnt signaling pathway as the most significantly altered pathway following GSK484 treatment. Given that VCL, β-catenin, and VE-cadherin form a complex critical for maintaining EC AJs, we investigated the impact of NETs inhibition on the Wnt signaling pathway, which is known to regulate these key proteins. Key components of this pathway, including *Wnt2, Wnt3, Wnt9a, β-catenin,* and *TCF4*, were selected for further analysis (mRNA expression is obtained from RNA-seq data

(See figure on next page.)

Fig. 6 The expression distribution of the top 1 modules associated proteins in the hippocampus. **A** Double labeling IF staining of VCL with microglia (Iba-1), astrocytes (GFAP), neurons (NeuN) and ECs (CD31) in the hippocampus (n = 6). **B** The colocalization analysis of VCL with Iba-1, GFAP, NeuN and CD31 by ImageJ (n = 6). **C** Double labeling IF staining of Fermt1 with microglia (Iba-1), astrocytes (GFAP), neurons (NeuN) and ECs (CD31) in the hippocampus (n = 6). **D** The colocalization analysis of Fermt1 with Iba-1, GFAP, NeuN and CD31 by ImageJ (n = 6). NETs: Neutrophil extracellular traps; CLP: Cecal Ligation and Puncture; SAE: Sepsis-associated encephalopathy; IF: immunofluorescence

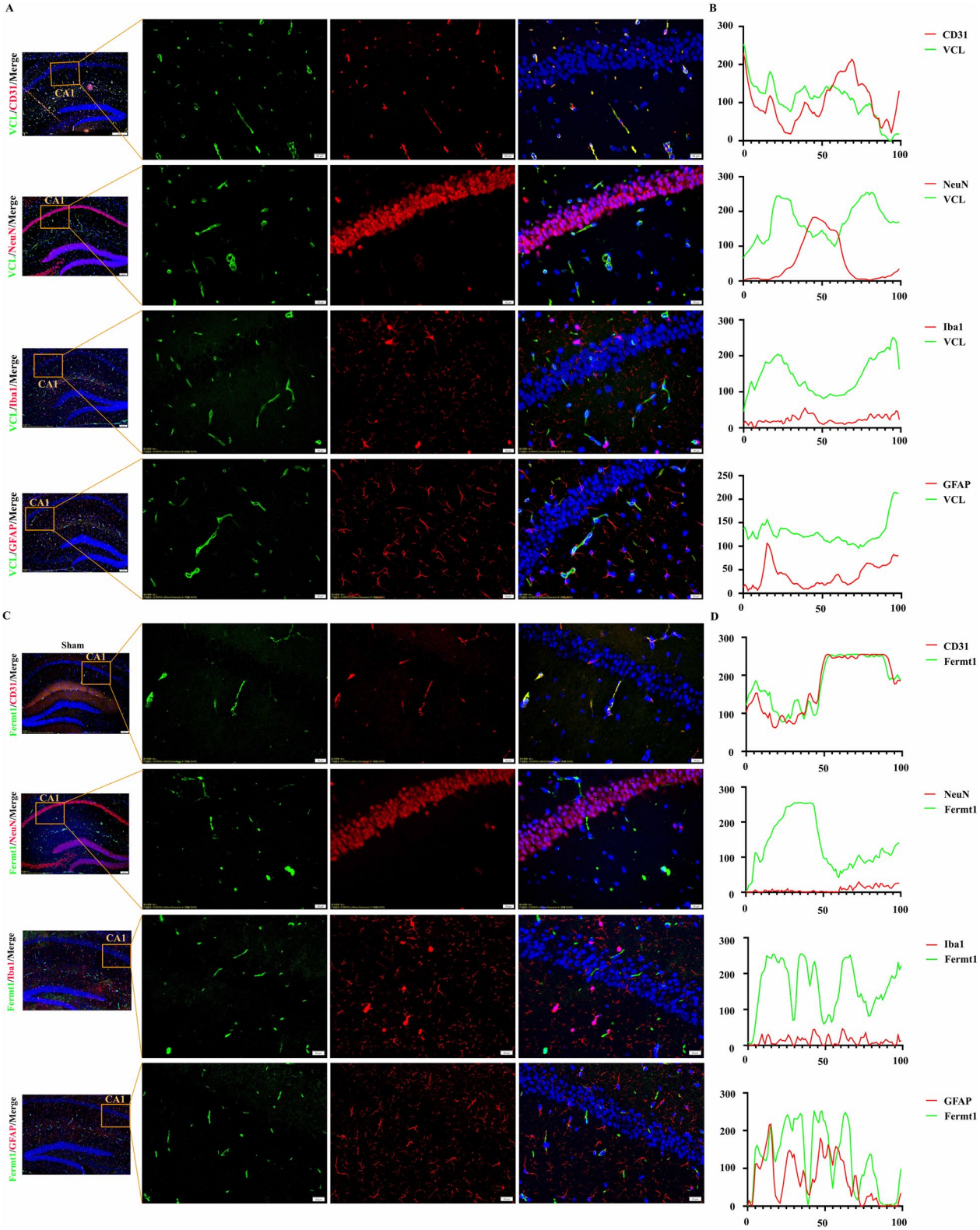

Fig. 6 (See legend on previous page.)

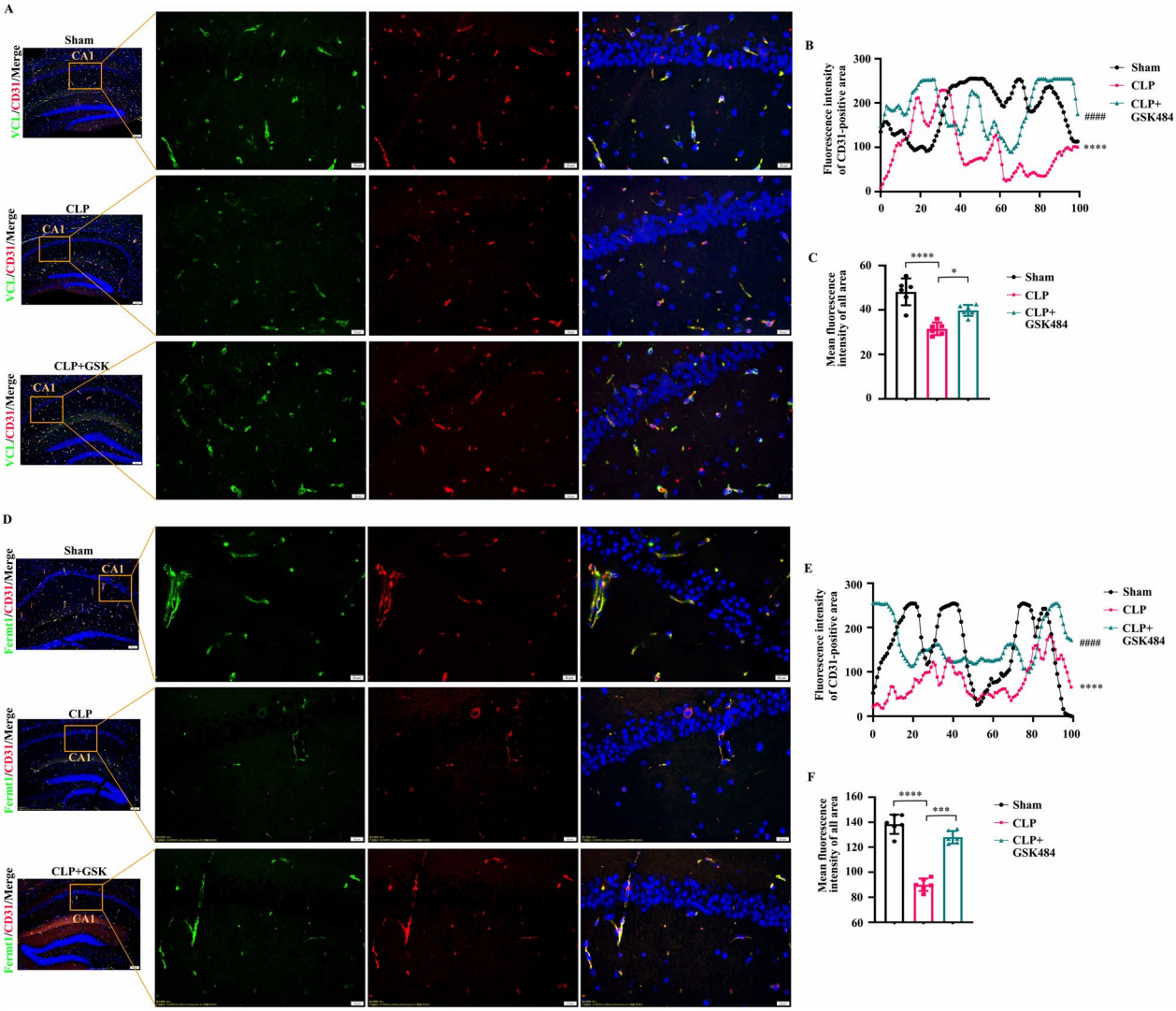

Fig. 7 The inhibition of NETs improved the top 1 modules associated proteins expression in the hippocampus. **A** Double labeling IF staining of VCL with ECs (CD31) after GSK484 treatment in the hippocampus (n = 6). **B** Quantification of the fluorescence intensity of VCL in CD31-positive area (n = 6). **C** Quantification of the mean fluorescence intensity of VCL in all area (n = 6). **D** Double labeling IF staining of Fermt1 with ECs (CD31) after GSK484 treatment in the hippocampus (n = 6). **E** Quantification of the fluorescence intensity of Fermt1 in CD31-positive area (n = 6). **F** Quantification of the mean fluorescence intensity of Fermt1 in all area (n = 6). NETs: Neutrophil extracellular traps; CLP: Cecal Ligation and Puncture; SAE: Sepsis-associated encephalopathy; IF: immunofluorescence. (*$p < 0.05$, ***$p < 0.001$, ****$p < 0.0001$; $^{\#\#\#}p < 0.001$, $^{\#\#\#\#}p < 0.0001$; *sham vs CLP, $^{\#}$CLP vs CLP + GSK484)

shown in Suppl. File. 2). To validate these findings, we assessed the protein expression levels of these components: Wnt2, Wnt3, Wnt9a, β-catenin, phosphorylated β-catenin (P-β-catenin), nuclear β-catenin and TCF4 (Fig. 9A). WB results showed that TCF4 expression was significantly downregulated in the CLP group compared to the sham group, whereas GSK484 treatment markedly restored TCF4 levels ($p < 0.05$, Fig. 9B), demonstrating the activation of the Wnt/β-catenin signaling pathway after GSK484 treatment. Interestingly, the total β-catenin levels did not differ significantly among the sham, CLP, and CLP + GSK484 groups (Fig. 9C). Further analysis of P-β-catenin (Fig. 9D) and nuclear β-catenin (Figs. 9E) revealed that nuclear β-catenin levels were decreased in the CLP group but significantly upregulated after GSK484 treatment. In contrast, P-β-catenin levels were increased in the CLP group but significantly reduced following GSK484 treatment. These findings suggest that GSK484 may regulate the dynamic balance between P-β-catenin and nuclear β-catenin. Since P-β-catenin

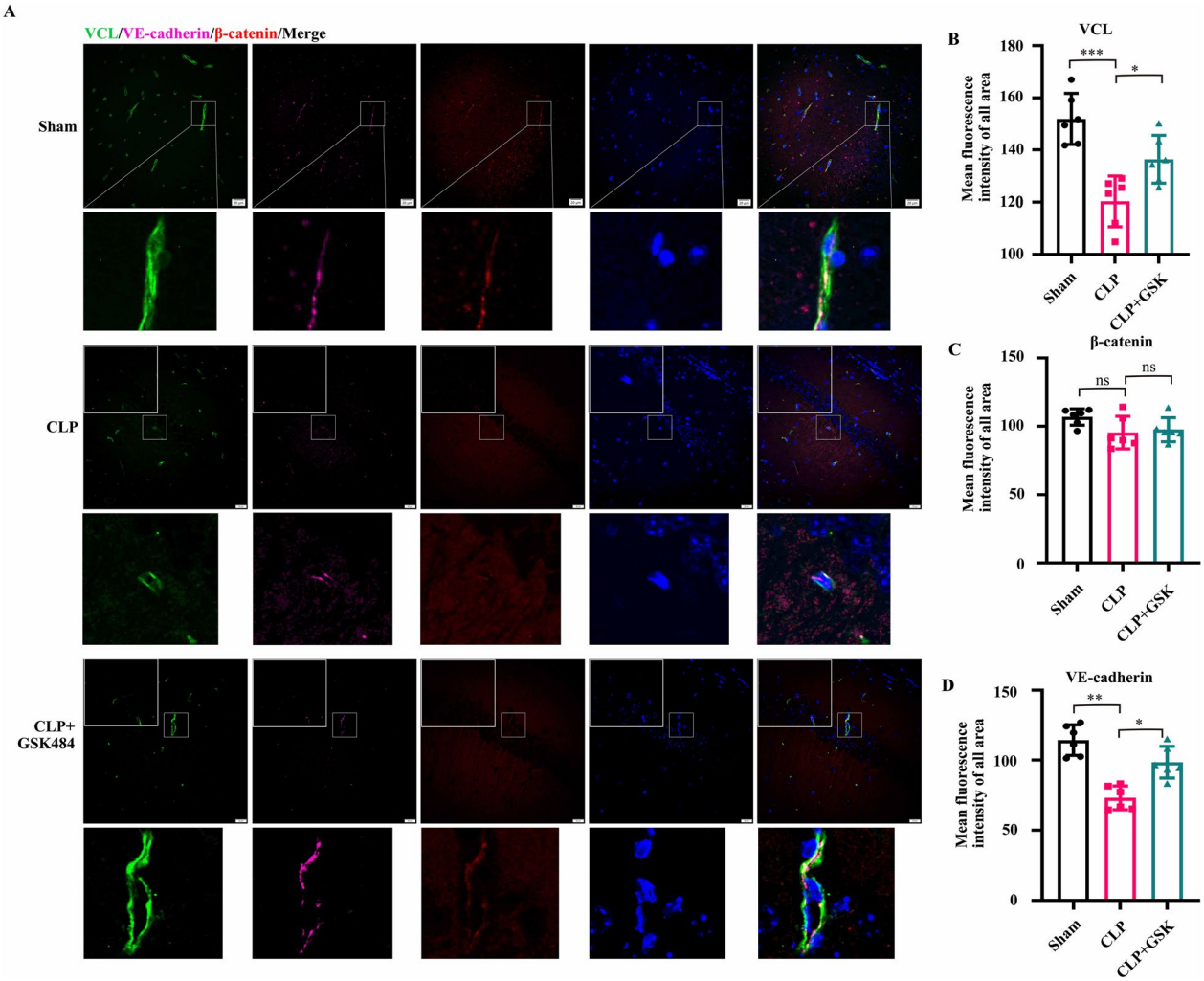

Fig. 8 The inhibition of NETs formation alleviated the AJs disruption may by regulating VCL/β-catenin/VE-cadherin functional complex. **A** Triple labeling IF staining showed colocalization of VCL, β-catenin and VE-cadherin (n = 6); Quantification of the fluorescence intensity of VCL (**B**), β-catenin (**C**) and VE-cadherin (**D**) in the hippocampus (n = 6). NETs: Neutrophil extracellular traps; CLP: Cecal Ligation and Puncture; SAE: Sepsis-associated encephalopathy; IF: immunofluorescence. (ns: no significance, *$p < 0.05$, **$p < 0.01$, ***$p < 0.001$)

inhibits Wnt signaling by limiting the availability of active β-catenin for nuclear translocation [46], the reduction in P-β-catenin levels induced by GSK484 likely facilitates β-catenin nuclear translocation, thereby restoring Wnt signaling activity and contributing to its downstream effects.

Next, we found that the expression of Wnt2 and Wnt9a have no significant changes among sham, CLP and CLP + GSK484 (Fig. 9F, G). However, Wnt3 expression was significantly downregulated in CLP group compared to the sham group, and GSK484 treatment markedly increased Wnt3 levels ($p < 0.05$, Fig. 9H). As, Wnt3 is a ligand of the Frizzled receptor. Therefore, we further investigated its expression and distribution to identify the cellular source of Wnt3 secretion in the hippocampus CA1 region of septic mice. And we found that Wnt3 is mainly expressed within neurons in the hippocampal CA1 region (Fig. 9I, J). These findings underscore the central role of the Wnt3/β-catenin/TCF4 axis in mediating the protective effects of NET inhibition on the BBB, particularly in maintaining the integrity of both TJs and AJs.

To explore the molecular mechanisms by which GSK484 regulates the integrity of cerebral ECs and the Wnt3/β-catenin/TCF4 signaling pathway, we first isolated bone marrow-derived neutrophils (NEs) from mice and induced NETs formation using PMA (100 nM). GSK484 treatment significantly reduced PMA-induced NETs formation ($p < 0.05$, Suppl. Figures 4A-4B). Subsequently, we established a co-culture model using a

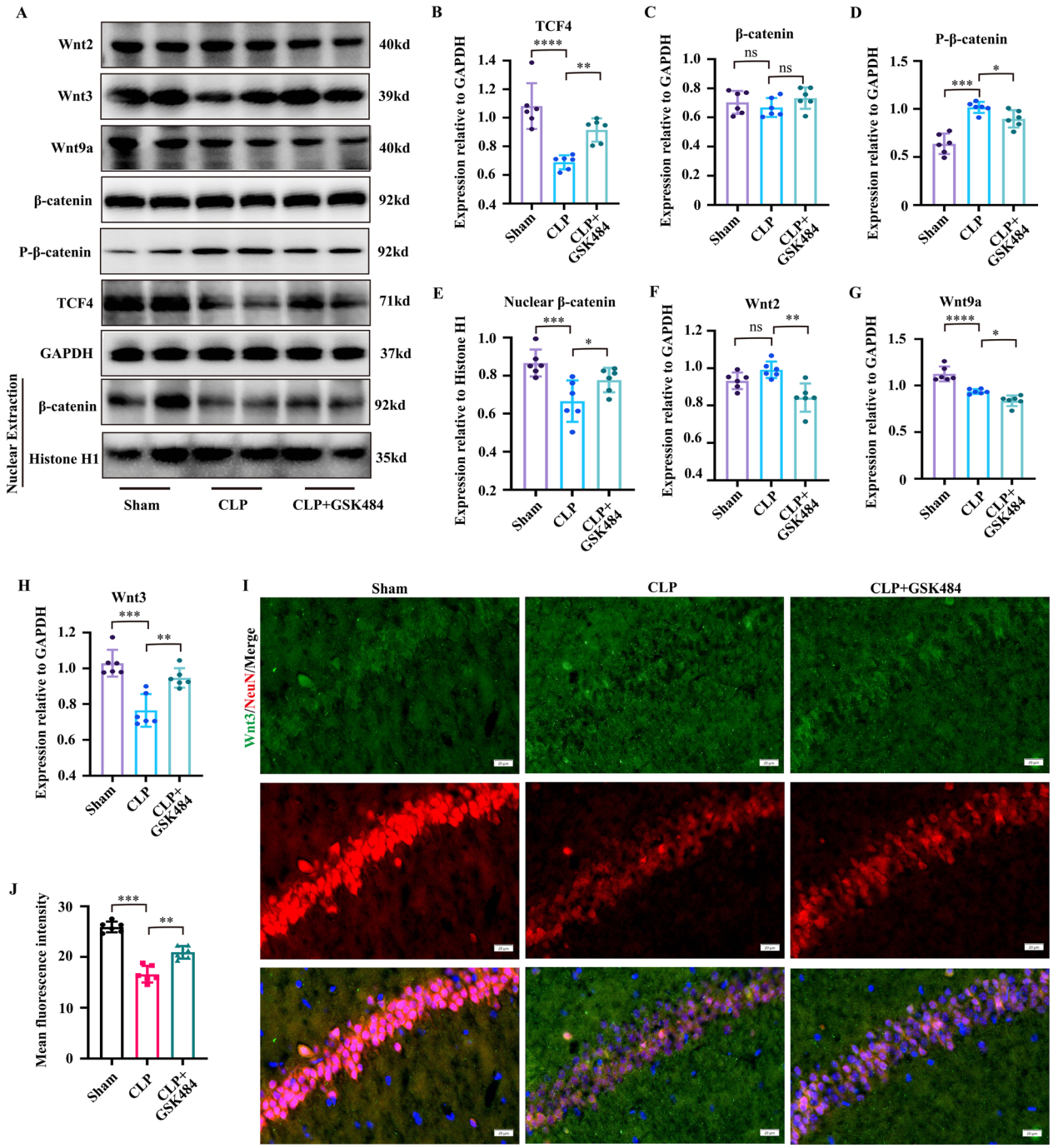

Fig. 9 The inhibition of NETs formation alleviated the disruption of TJs and AJs by activating Wnt3/β-catenin/TCF4 signaling pathway. **A** Expression levels of Wnt/β-catenin/TCF4 signaling proteins in the hippocampus were detected by Western blot (n = 6). **B**–**H** The quantification analysis of Wnt/β-catenin/TCF4 signaling proteins expression levels (n = 6). **I** Wnt3 is predominantly secreted by neurons in the hippocampal CA1 region of septic mice. **J** Quantification of the mean fluorescence intensity of Wnt3 in CA1 region (n = 6). NETs: Neutrophil extracellular traps; CLP: Cecal Ligation and Puncture; SAE: Sepsis-associated encephalopathy; BBB: Blood–brain barrier; TJs: Tight junctions; AJs: adherens junction (ns: no significance, *$p < 0.05$, **$p < 0.01$, ***$p < 0.001$, ****$p < 0.0001$)

Transwell™ system, with NEs seeded in the upper chamber and bEnd.3 cells in the lower chamber. In this system, PMA-induced NETs formation by NEs simulated the interaction between NETs and ECs. Our results demonstrated that NETs formation in the co-culture system significantly suppressed the β-catenin/TCF4 signaling pathway in bEnd.3 cells, indicating that NETs negatively regulate this pathway at the cellular level. Interestingly, while GSK484 treatment alone showed limited activation of the β-catenin/TCF4 pathway, the addition of exogenous Wnt3 significantly restored its activation. Notably, the combined treatment with Wnt3 and GSK484 resulted in an even greater activation of the β-catenin/TCF4 pathway, surpassing the effects of Wnt3 alone ($p < 0.05$, Suppl. Figures 4C-4G). These findings suggest that GSK484 enhances β-catenin/TCF4 signaling in ECs in a Wnt3-dependent manner, offering new insights into the role of NETs inhibition in preserving endothelial function in vitro.

LF3-mediated inhibition of β-catenin/TCF4 signaling reverses GSK484-induced protection of BBB integrity and cognitive function

To further confirm the role of Wnt/β-catenin/TCF4 signaling in regulating the TJs and AJs integrity after NETs inhibition, we treated CLP + GSK484 mice with LF3, an antagonist of β-catenin/TCF4 signaling, via intracerebroventricular (i.c.v.) administration. LF3 disrupted Wnt signaling by inhibiting the interaction between β-catenin and TCF4. WB analysis (Fig. 10A–C) revealed that LF3 treatment significantly decreased Wnt3 and TCF4 expression in the CLP + GSK484 + LF3 group compared to the CLP + GSK484 group. Similarly, nuclear β-catenin levels were reduced in the LF3-treated group (Fig. 10D), though total β-catenin levels remained unchanged (Fig. 10E). Notably, P-β-catenin expression was reversed by LF3 treatment (Fig. 10F), suggesting that blocking β-catenin/TCF4 signaling reinstated P-β-catenin-mediated inhibition of Wnt signaling.

Next, we examined the expression levels of TJ and AJ proteins following LF3 treatment. The results showed that LF3 administration reduced the expression of ZO-1, Occludin, VCL, MSN, VE-cadherin, and Fermt1 in the CLP + GSK484 mice (Fig. 10G–M). To evaluate cognitive function following LF3 treatment, we conducted the OFT and MWM test. The results revealed that mice in the CLP + GSK484 + LF3 group showed a significantly reduced movement distance and spent less time in the center area during the OFT (Suppl. Figures 5A-5C) compared to the CLP + GSK484 group. Similarly, in the MWM test, the CLP + GSK484 + LF3 group exhibited worsened performance (Suppl. Figures 5D-5F), indicating that inhibition of β-catenin/TCF4 signaling counteracted the cognitive improvements induced by GSK484 in CLP mice. These findings suggest that inhibiting NET formation preserved the integrity of TJs and AJs, as well as cognitive function, primarily through the activation of the Wnt3/β-catenin/TCF4 signaling pathway.

Discussion

NETs formation has been reported to be a potential target for treating early brain injury in CNS disease [15, 24], though few studies have examined its role in SAE. In this study, we aimed to further investigate the contribution of NETs to SAE progression and elucidate the underlying mechanisms (Fig. 11). We observed the following findings. (1) The expression level of NETs was significantly increased in mice and peaked at 72 h in the brain post-CLP modeling. (2) Pharmacological inhibition of NETs formation significantly alleviated CLP-induced neuroinflammation response, BBB damage, and cognitive dysfunction. (3) inhibiting NETs formation significantly alleviated BBB damage by upregulating Occludin expression in TJs and promoting the VCL/β-catenin/VE-cadherin complex in AJs; and (4) the Wnt3/β-catenin/TCF4 signaling pathway was involved in protecting TJs and AJs following NETs inhibition.

SAE is a systemic inflammatory response induced by sepsis resulting in brain BBB injury and diffuse neuroinflammatory response [5], yet its pathogenesis remains unclear. In this study, we employed the classical CLP model to induce sepsis in mice and investigate SAE pathogenesis [28]. Previous research by Zhu et al. highlighted the critical roles of neutrophils and NETs in CLP-induced cognitive impairment and BBB permeability [11]. However, their research primarily focused on inhibiting NETs formation and reducing neutrophil activation, without fully exploring the downstream protective mechanisms of NETs inhibition. Our study addressed this gap by administering GSK484 and employing RNA-seq to assess hippocampal RNA expression changes post-treatment. Additionally, we provided the first detailed timeline of neutrophils infiltration and NETs formation in SAE mice, underscoring their pivotal role in the disease's pathogenesis. Through our study, we also evaluated the protective effects of GSK484 in mitigating SAE severity.

Neutrophils, as the first line of innate immune defense, combat infection through phagocytosis and inflammatory cytokine release, while also forming NETs to trap pathogens [12]. However, excessive neutrophil activation and NETs formation exacerbate inflammation and damage [7, 12], as observed in neuroinflammatory conditions like stroke [47, 48], traumatic brain injury [49], and sepsis [11, 17]. In sepsis, elevated circulating NETs are associated with poor outcomes, including organ failure, thrombocytopenia, coagulopathy, and increased

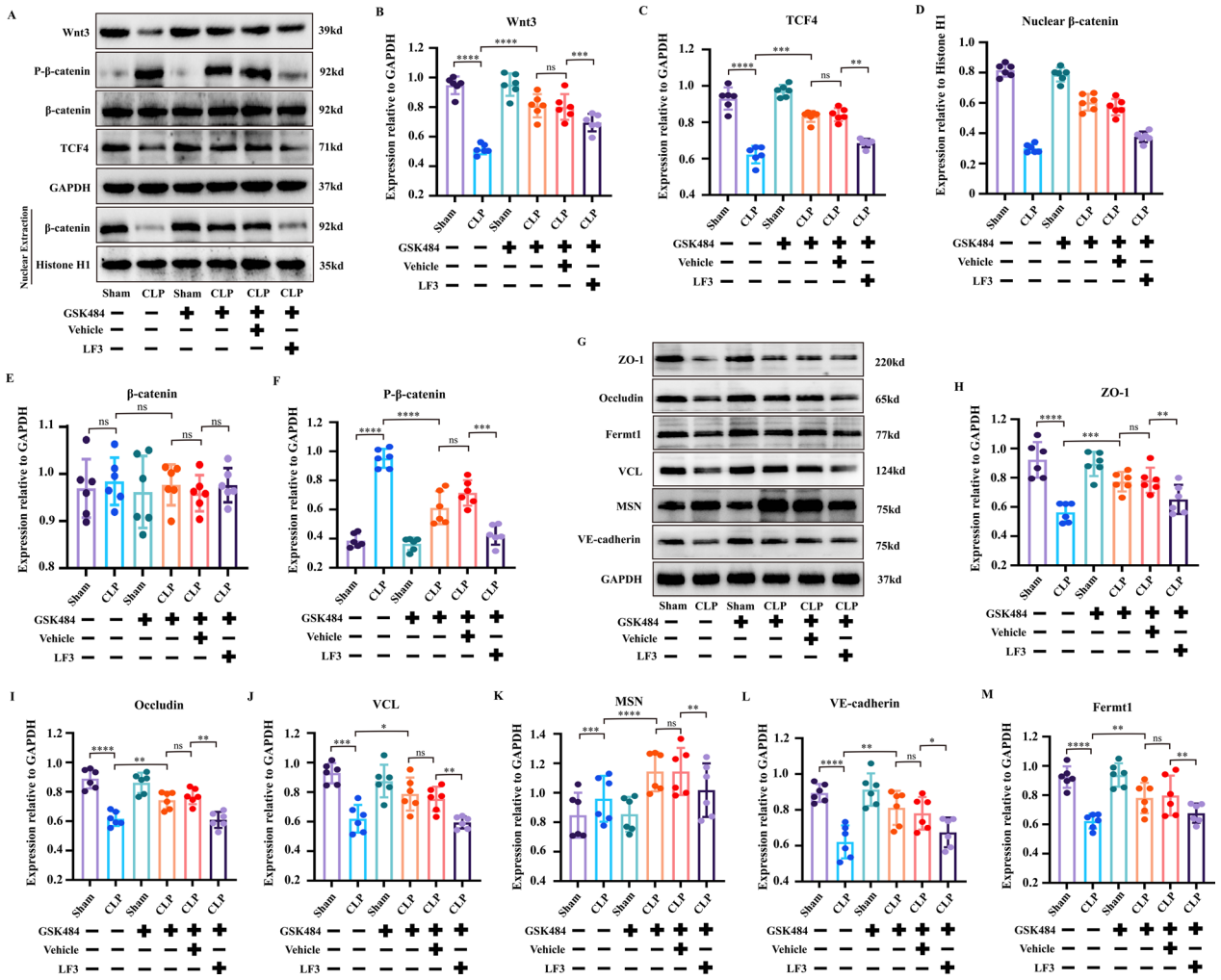

Fig. 10 The LF3 treatment reversed the expression of Wnt3/β-catenin/TCF4 signaling pathway, TJs and AJs proteins. **A** Western blot detected the Wnt/β-catenin/TCF4 signaling proteins expression levels in the hippocampus after LF3 treatment (n = 6). **B**–**F** The quantification analysis of Wnt/β-catenin/TCF4 signaling proteins expression levels after LF3 treatment (n = 6). **G** Western blot detected the TJs and AJs proteins expression levels in the hippocampus after LF3 treatment (n = 6). **H**–**M** The quantification analysis of TJs and AJs proteins expression levels after LF3 treatment (n = 6). NETs: Neutrophil extracellular traps; CLP: Cecal Ligation and Puncture; SAE: Sepsis-associated encephalopathy; BBB: Blood–brain barrier; TJs: Tight junctions; AJs: adherens junction (ns: no significance, *$p < 0.05$, **$p < 0.01$, ***$p < 0.001$, ****$p < 0.0001$)

mortality [17, 50]. Higher NET-forming capacity has been linked to disseminated intravascular coagulation (DIC) and 28-day mortality, while increased MPO-DNA levels are associated with hypotension, oxygenation impairment, and higher SOFA scores [51]. These findings highlight the promise and translational potential of therapeutic strategies targeting NETs in sepsis. The ongoing trial (NCT05453695), investigating the safety and efficacy of DNase in reducing organ dysfunction and ICU stay, underscores the clinical relevance of NET inhibition [52]. Similarly, reparixin, a CXCR1/2 inhibitor, has demonstrated efficacy in reducing NET formation and fibrin deposition in septic lungs [53], Cl-amidine, a PAD4 inhibitor currently in clinical trials for diabetes, further illustrates the potential of targeting NETs in inflammatory diseases [54]. In this context, GSK484, a novel PAD4 inhibitor, stands out as a promising candidate. Although research on GSK484 remains limited, its ability to inhibit NET formation and protect against neuroinflammation and BBB damage positions it as a potential therapeutic option for sepsis and related disorders (Such as SAE). These findings warrant further investigation into its therapeutic potential.

Utilizing RNA-seq data, we identified DEGs and their interactions through the STRING database, pinpointing the top 10 most significant hub genes. Among these, we

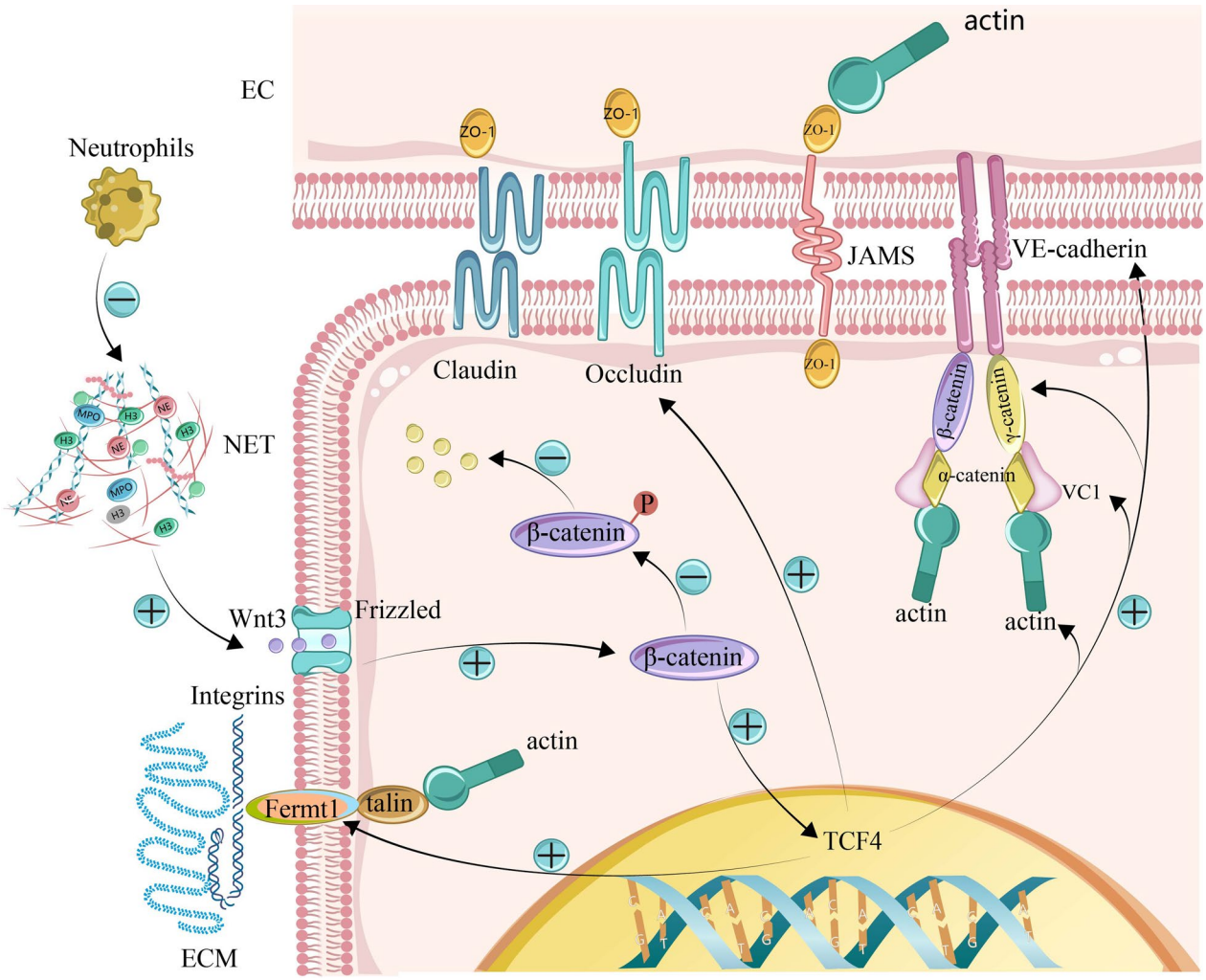

Fig. 11 Mechanism diagram illustrating how NETs affect endothelial cell barrier function by activating the Wnt3/β-catenin/TCF4 signaling pathway

focused on five key hub genes: *VCL, Cldn11, MSN, Ocln,* and *Fermt1*, all of which play roles in the formation of TJs, AJs and cellular structure. We conducted a detailed analysis of the expression and function of these genes and their corresponding proteins in the SAE model. As previously mentioned, Occludin, ZO-1, and Claudins are the primary components of TJs [55]. Therefore, the observed increase in Occludin expression following GSK484 treatment suggests a potential enhancement in BBB permeability in the SAE model. While Claudin-11, encoded by the *Cldn11* gene, was also investigated as another TJs protein in this context. It primarily functions to establish an electrically tight barrier in myelinated nerves, where it is a major component of CNS myelin [38]. Unlike other TJs proteins, Claudin-11's role is more closely associated with the physical properties of myelin rather than with BBB integrity. As such, its impact on BBB permeability is limited. In humans, *Cldn11* variants have been linked to mild intellectual impairments [56], but its primary function remains within myelin, where it accounts for approximately 7% of the total protein composition. Interestingly, *Cldn11* knockout mice exhibit mild neurological deficits, such as body tremors, hindlimb weakness, and behavioral abnormalities, but no impairment in myelin formation [37, 57]. In the context of SAE, GSK484 treatment resulted in a reduction of Claudin-11 expression in neuronal cell. However, given its limited role in BBB integrity and cognitive function, this change is unlikely to have a significant impact. Instead, the observed upregulation of Occludin and other TJs components following GSK484 treatment underscores its therapeutic potential in enhancing BBB permeability and mitigating neuroinflammation in SAE.

MSN is a member of ezrin/radixin/moesin family, which plays an essential role in the control of cellular morphology, adhesion, and motility by linking actin

cytoskeleton to membrane [43]. In hepatocellular carcinoma cells, MSN overexpression increased invadopodia formation, improved the expressions of β-catenin and its downstream factors, and also enhanced the nuclear translocation of β-catenin [58]. Furthermore, high MSN expression activated the Wnt/β-catenin pathway and resulted in aggressive glioblastoma development in mice [59]. These results showed that MSN has also been related to the activation of Wnt/β-catenin pathway. In our study, GSK484 treatment increased the expression of MSN in both mRNA and protein levels, but this increase has no sharply different in the CD31-positive area. Therefore, the MSN might not support brain ECs cellular structural remodeling, cell adhesion or Wnt//β-catenin activation in CLP-induced SAE model, and the detailed role of MSN in brain of SAE mice are needed to further explore.

Another significant hub gene, Fermt1, encodes a member of the fermitin family, and contains a FERM domain and a pleckstrin homology domain [60]. Its encoded protein is involved in integrin signaling and linkage of the actin cytoskeleton to the ECM. In colon cancer, Fermt1 interacted directly with β-catenin and activated the Wnt/β-catenin signaling pathway by decreasing the phosphorylation level of β-catenin, enhancing β-catenin nuclear translocation and increasing the transcriptional activity of β-catenin/TCF/LEF [61]. Which indicated that Fermt1 is not only a protein that regulates cell adhesion, but also a positive regulator of Wnt signaling. Our data found that Fermt1 expression in the brain is mainly located in ECs, and GSK484 treatment significantly increase its expression. Therefore, we speculated that Fermt1 may involve in improving the adhesion between brain ECs and ECM, coupled with activation of Wnt/β-catenin signaling pathway after inhibiting NETs.

VCL, a highly conserved cytoplasmic protein and a key component of cortical scaffolding, is critical for cell–cell adhesion and the function of AJs [62]. It localizes to specific adhesion sites with the help of various binding partners, including talin and α-catenin, which target VCL to integrin and cadherin complexes, respectively, as well as α-actinin and β-catenin [62]. β-catenin, a submembrane protein, connects the cytoplasmic domains of cadherins to the actin cytoskeleton through α-catenin [35]. In vitro binding assays have shown a direct interaction between β-catenin and VCL, which facilitates the mitigation of excess tension and stabilizes the cadherin-catenin complex, thereby strengthening the link between the cytoskeleton and the cell cortex [44]. VE-cadherin, the first endothelial-specific cadherin molecule, also interacts with β-catenin, a relationship crucial for regulating vascular permeability [55, 63]. During inflammatory injury, inflammatory agents can transiently disrupt the VE-cadherin/β-catenin complex [64]. Conversely, the mechanisms of dissociation and subsequent reassociation of VE-cadherin/β-catenin play a critical role in restoring normal barrier function following exposure to acute inflammatory mediators [64]. Our triple labeling experiments revealed colocalization of VCL, β-catenin, and VE-cadherin, suggesting that VCL may form a complex with VE-cadherin and β-catenin, playing a crucial role in stabilizing their interaction and thereby preserving BBB integrity.

Previous studies have indicated that activation of the Wnt/β-catenin pathway can specifically induce the expression of TJs and AJs proteins transcription factors in brain ECs [65–67]. Our RNA-seq and WB results showed that activation of the Wnt/β-catenin/TCF signaling pathway increases the expression of Occludin, VCL, and Fermt1 at both the mRNA and protein levels. Notably, GSK484 treatment elevated the protein levels of VE-cadherin, although no significant change in VE-cadherin mRNA expression was observed. Our previous research demonstrated that the expression levels of matrix metalloproteinase 2/9 (MMP2/9) in hippocampal tissue were upregulated after CLP surgery [46], and it is well-established that MMPs can degrade both TJs and AJs proteins [68, 69]. Moreover, activation of Wnt signaling has been reported to lower the degradation of VE-cadherin [67]. Therefore, we proposed that Wnt/β-catenin/TCF4 signaling regulates VE-cadherin protein expression, possibly by reducing its degradation rather than through transcriptional activation, particularly in the context of CLP-induced neuroinflammation.

Our bioinformatics analysis and WB results identified the Wnt3/β-catenin/TCF4 signaling pathway as the most significant signaling pathway activated by GSK484 treatment. Wnt/β-catenin signaling is fundamental in CNS vascularization, BBB formation, and maturation during embryonic and postnatal development [70, 71]. In the CNS, astrocytes, neurons and oligodendrocytes secrete Wnt ligands, such as Wnt2, Wnt3, Wnt3a and Wnt7. These ligands bind to Frizzled receptor complexes on ECs, stabilizing and activating Wnt/β-catenin signaling [72]. Activation of this pathway strengthens endothelial AJs and TJs, decreases transendothelial vesicular trafficking, and induces specific transporters for the delivery of essential nutrients to the CNS [70, 71, 73]. Several research found that inhibiting Wnt/β-catenin signaling aggravates BBB breakdown and lead to hemorrhagic transformation in mouse ischemic stroke model [74, 75]. Conversely, pharmacological or genetic activation of Wnt/β-catenin signaling has been found to repair BBB damage and reduce hemorrhagic defects following ischemic stroke [72, 74, 76]. These findings suggest that Wnt/β-catenin signaling activation plays a protective role

in maintaining BBB integrity during acute neuroinflammation-induced brain injury, which is consistent with our results.

β-catenin serves a dual role as both an AJs protein that links to the actin cytoskeleton and as a key transcription factor in the Wnt signaling [77]. When endothelial AJs are disrupted, β-catenin is released from the plasma membrane, leading to its transcriptional activity [78]. And the increased expression of β-catenin binds to TCF transcription factors in the nucleus, thereby activating Wnt signaling [79]. However, our findings indicated that total β-catenin protein levels did not significantly differ among the sham, CLP, and CLP + GSK484 groups. In contrast, nuclear β-catenin levels were significantly downregulated in the CLP group compared to the sham group, and GSK484 treatment effectively reversed this decrease. Additionally, we observed a significant increase in P-β-catenin in the CLP group compared to the sham group. As reported by Lilien et al., β-catenin phosphorylation disrupts its interaction with VE-cadherin in AJs, leading to complex dissociation and β-catenin release [80]. P-β-catenin is unstable and prone to degradation [81], and its presence reduces the amount of active β-catenin available to enter the nucleus, thereby inhibiting Wnt signaling activation [46]. Our results suggest that GSK484 treatment reduces P-β-catenin levels, allowing for an increase in active β-catenin in the cytoplasm, which facilitates its transport to the nucleus and membrane, ultimately promoting Wnt signaling activation.

Nevertheless, this study several limitations. First, while previous studies have explored the mechanisms of NETs release and the protective effects of DNase I on SAE [11], our study used GSK484 to inhibit NETs formation without testing DNase I or Cl-amidine in CLP mice. Second, although we partially uncovered the protective mechanism of NETs inhibition by GSK484, the precise mechanism by which NETs regulate Wnt signaling remains unclear. While we demonstrated how Wnt signaling regulates BBB permeability by promoting Occludin expression and VCL/β-catenin/VE-cadherin complex formation in an animal model, we were unable to show how NETs influence this complex at the cellular level. Further research is needed to clarify the relationships and mechanisms among NETs, BBB integrity, and Wnt signaling through multi-dimensional experimental approaches.

Conclusions

NETs gave rise to inflammatory injury following CLP. Pharmacological inhibition of NETs significantly alleviated the CLP-induced neuroinflammation response, BBB damage and cognitive dysfunction. The protect effect of NETs inhibition on BBB is primarily mediated through increased Occludin expression and the formation of the VCL/β-catenin/VE-cadherin complex, facilitated by the activation of the Wnt3/β-catenin/TCF4 signaling pathway. Thus, NETs may serve as a novel therapeutic target for CLP-induced SAE and offer a promising strategy for SAE treatment.

Abbreviations

SAE	Sepsis-associated encephalopathy
NETs	Nneutrophil extracellular traps
RNA-Seq	RNA sequencing
BBB	Blood–brain barrier
CLP	Cecal ligation puncture
CNS	Central nervous system
BWC	Brain water content
FS	Fluorescein sodium
MPO	Myeloperoxidase
ECs	Endothelial cells
PAMPs	Pathogen-associated molecular patterns
DAMPs	Damage-associated molecular patterns
TJs	Tight junctions
AJs	Adherens junctions
JAMs	Junction adhesion molecules
PAD4	Protein arginine deiminase 4
IF	Immunofluorescence
PMA	Pphorbol 12-myristate 13-acetate
MWM	Morris water maze
OFT	Open field test
WB	Western blot
DEGs	Differentially expressed genes
GO	Gene ontology
KEGG	Kyoto Encyclopedia of Genes and Genomes
PPIs	Protein–protein interactions
MMP	Matrix metalloproteinase
ECM	Extracellular matrix

Supplementary Information

The online version contains supplementary material available at https://doi.org/10.1186/s12974-025-03395-6.

Supplementary Material 1.

Supplementary Material 2.

Supplementary Material 3: Supplementary Fig. 1 Effects of GSK484 treatment on Claudin-11 expression in brain of SAE mice and the expression of Occludin in bEnd.3 cells. A. Western blot detected the Claudin-11 proteins expression levels in brain (n=6). B. The quantification analysis of Claudin-11 proteins expression in brain (n=6). C. IF staining shows expression and distribution of Claudin-11 in the CA1 region of the hippocampus (40x, n=6). D. Quantification of the fluorescence intensity and distribution of Occludin in bEnd.3 cells. E. IF staining shows expression and distribution of Occludin in bEnd.3 cells. IF: immunofluorescence. (ns: no significance, * p <0.05, ** p <0.01, *** p <0.001, **** p <0.0001).

Supplementary Material 4: Supplementary Fig. 2 The expression patterns of MSN in brain cell types. A. Double labeling IF staining of MSN with microglia (Iba-1), astrocytes (GFAP), neurons (NeuN) and ECs (CD31) in the hippocampus (n=6). B. The colocalization analysis of MSN with Iba-1, GFAP, NeuN and CD31 by ImageJ (n=6). NETs: Neutrophil extracellular traps, CLP: Cecal Ligation and Puncture, SAE: Sepsis-associated encephalopathy, IF: immunofluorescence.

Supplementary Material 5: Supplementary Fig. 3 MSN expression is elevated in the CLP group and partially affected by GSK484 treatment. A. Double labeling IF staining of MSN with ECs (CD31) after GSK484 treatment in the hippocampus (n=6). B. Quantification of the mean fluorescence intensity of MSN in all area (n=6). C. Quantification of the fluorescence intensity of MSN in CD31-positive area (n=6). NETs: Neutrophil extracellular traps, CLP: Cecal Ligation and Puncture, SAE:

Sepsis-associated encephalopathy, IF: immunofluorescence. (* p <0.05, ** p <0.01, *** p <0.001, **** p <0.0001; *: sham vs CLP, ^{ns}: CLP vs CLP+GSK484).

Supplementary Material 6: Supplementary Fig. 4 GSK484 enhances β-catenin/TCF4 signaling in ECs through Wnt3-dependent mechanisms in vitro. A. Representative photographs of IF staining of Cit-H3/MPO/DAPI in PMA-treated NE; B. The quantification of the number of Cit-H3/MPO/DAPI+ cells (n=3). C. Western blot detected the β-catenin/TCF4 signaling proteins expression levels in bEnd.3 cell (n=3). D-G. The quantification analysis of Wnt/β-catenin/TCF4 signaling proteins expression in bEnd.3 cell (n=3). NE: Neutrophil, EC: Endothelial cell, Cit-H3: Citrullinated histones H3, MPO: Myeloperoxidase, IF: immunofluorescence. (ns: no significance, * p <0.05, ** p <0.01, *** p <0.001, **** p <0.0001).

Supplementary Material 7: Supplementary Fig. 5 The β-catenin/TCF4 inhibitor, LF3, reversed the cognitive improvements induced by GSK484 in CLP mice. A. The trace heat map of OFT. The time (B) and the movement distance (C) in center in OFT. D. The trace heat map of MWM test. The movement distance (E) in island, and the time (F) in NW area in the MWM test were increased after GSK484 treatment (n=6). CLP: Cecal Ligation and Puncture, OFT: open field test, MWM: Morris water maze. (ns: no significance, * p <0.05, ** p <0.01, *** p <0.001, **** p <0.0001).

Supplementary Material 8.

Acknowledgements
Not applicable.

Author contributions
Jianhe Yue designed the experiments and drafted the manuscript. Jianhe Yue, Ning Huang and Yuan Cheng provided research funding. Lijuan Mo, Guotao Zeng and Yuhang Peng performed the experiments; Ping Ma, Xiaolin Zhang and Xiang Zhang acquired and collected the data; Yongxiang Jiang, You Zhou and Ning Huang analyzed and verified the data; Yuan Cheng and Ning Huang conceived the idea and edited the manuscript.

Funding
This work was supported by the China Postdoctoral Science Foundation (Certificate Number: 2024M753878), Project of Second Affiliated Hospital of Chongqing Medical University (kryc-yq-2216), Chunhui Project Foundation of the Education Department of China (HZKY20220218) and Joint Project of Pinnacle Disciplinary Group, the Second Affiliated Hospital of Chongqing Medical University (2024310).

Availability of data and materials
No datasets were generated or analysed during the current study.

Declarations

Ethics approval and consent to participate
All animal experimental procedures were conducted in accordance with the animal care regulations of the Institutional Animal Care and Use Committee of the Second Affiliated Hospital of Chongqing Medical University.

Consent for publication
Not applicable.

Competing interests
The authors declare no competing interests.

Author details
[1]Joint Project of Pinnacle Disciplinary Group, The Second Affiliated Hospital of Chongqing Medical University, Chongqing, China. [2]Department of Neurosurgery, The Second Affiliated Hospital of Chongqing Medical University, Chongqing, China. [3]Department of Neurology, The Second Affiliated Hospital of Chongqing Medical University, Chongqing, China. [4]Department of Critical Care Medicine, The Second Affiliated Hospital of Chongqing Medical University, Chongqing, China.

Received: 22 October 2024 Accepted: 23 February 2025
Published online: 18 March 2025

References

1. Chiu C, Legrand M. Epidemiology of sepsis and septic shock. Curr Opin Anaesthesiol. 2021;34:71–6.
2. Rudd KE, Johnson SC, Agesa KM, Shackelford KA, Tsoi D, Kievlan DR, Colombara DV, Ikuta KS, Kissoon N, Finfer S, et al. Global, regional, and national sepsis incidence and mortality, 1990–2017: analysis for the Global Burden of Disease Study. Lancet. 2020;395:200–11.
3. Ackerman MH, Ahrens T, Kelly J, Pontillo A. Sepsis. Crit Care Nurs Clin North Am. 2021;33:407–18.
4. Molnár L, Fülesdi B, Németh N, Molnár C. Sepsis-associated encephalopathy: a review of literature. Neurol India. 2018;66:352–61.
5. Hong Y, Chen P, Gao J, Lin Y, Chen L, Shang X. Sepsis-associated encephalopathy: from pathophysiology to clinical management. Int Immunopharmacol. 2023;124:110800.
6. Gao Q, Hernandes MS. Sepsis-associated encephalopathy and blood–brain barrier dysfunction. Inflammation. 2021;44:2143–50.
7. Mulet M, Osuna-Gómez R, Zamora C, Artesero I, Arús M, Vera-Artazcoz P, Cordón A, Vilalta N, San-José P, Abril A, et al. Dysregulated neutrophil extracellular traps formation in sepsis. Immunology. 2023;170:374–87.
8. Wang Y, Jin H, Wang W, Wang F, Zhao H. Myosin1f-mediated neutrophil migration contributes to acute neuroinflammation and brain injury after stroke in mice. J Neuroinflamm. 2019;16:77.
9. Zhao Z, Pan Z, Zhang S, Ma G, Zhang W, Song J, Wang Y, Kong L, Du G. Neutrophil extracellular traps: a novel target for the treatment of stroke. Pharmacol Ther. 2023;241:108328.
10. Hidalgo A, Libby P, Soehnlein O, Aramburu IV, Papayannopoulos V, Silvestre-Roig C. Neutrophil extracellular traps: from physiology to pathology. Cardiovasc Res. 2022;118:2737–53.
11. Zhu CL, Xie J, Liu Q, Wang Y, Li HR, Yu CM, Li P, Deng XM, Bian JJ, Wang JF. PD-L1 promotes GSDMD-mediated NET release by maintaining the transcriptional activity of Stat3 in sepsis-associated encephalopathy. Int J Biol Sci. 2023;19:1413–29.
12. Zhang H, Wang Y, Qu M, Li W, Wu D, Cata JP, Miao C. Neutrophil, neutrophil extracellular traps and endothelial cell dysfunction in sepsis. Clin Transl Med. 2023;13: e1170.
13. Mi L, Min X, Shi M, Liu L, Zhang Y, Zhu Y, Li P, Chai Y, Chen F, Deng Q, et al. Neutrophil extracellular traps aggravate neuronal endoplasmic reticulum stress and apoptosis via TLR9 after traumatic brain injury. Cell Death Dis. 2023;14:374.
14. Smyth LCD, Murray HC, Hill M, van Leeuwen E, Highet B, Magon NJ, Osanlouy M, Mathiesen SN, Mockett B, Singh-Bains MK, et al. Neutrophil-vascular interactions drive myeloperoxidase accumulation in the brain in Alzheimer's disease. Acta Neuropathol Commun. 2022;10:38.
15. Shafqat A, Noor Eddin A, Adi G, Al-Rimawi M, Abdul Rab S, Abu-Shaar M, Adi K, Alkattan K, Yaqinuddin A. Neutrophil extracellular traps in central nervous system pathologies: a mini review. Front Med. 2023;10:1083242.
16. Papayannopoulos V. Neutrophil extracellular traps in immunity and disease. Nat Rev Immunol. 2018;18:134–47.
17. Maneta E, Aivalioti E, Tual-Chalot S, Emini Veseli B, Gatsiou A, Stamatelopoulos K, Stellos K. Endothelial dysfunction and immunothrombosis in sepsis. Front Immunol. 2023;14:1144229.
18. Aslankoc R, Savran M, Ozmen O, Asci S. Hippocampus and cerebellum damage in sepsis induced by lipopolysaccharide in aged rats-Pregabalin can prevent damage. Biomed Pharmacother. 2018;108:1384–92.
19. Mei B, Li J, Zuo Z. Dexmedetomidine attenuates sepsis-associated inflammation and encephalopathy via central α2A adrenoceptor. Brain Behav Immun. 2021;91:296–314.
20. Manda-Handzlik A, Demkow U. The brain entangled: the contribution of neutrophil extracellular traps to the diseases of the central nervous system. Cells. 2019;8:1477.
21. Vossenaar ER, Zendman AJ, van Venrooij WJ, Pruijn GJ. PAD, a growing family of citrullinating enzymes: genes, features and involvement in disease. BioEssays. 2003;25:1106–18.

22. György B, Tóth E, Tarcsa E, Falus A, Buzás EI. Citrullination: a posttranslational modification in health and disease. Int J Biochem Cell Biol. 2006;38:1662–77.
23. Darrah E, Rosen A, Giles JT, Andrade F. Peptidylarginine deiminase 2, 3 and 4 have distinct specificities against cellular substrates: novel insights into autoantigen selection in rheumatoid arthritis. Ann Rheum Dis. 2012;71:92–8.
24. Zeng H, Fu X, Cai J, Sun C, Yu M, Peng Y, Zhuang J, Chen J, Chen H, Yu Q, et al. Neutrophil extracellular traps may be a potential target for treating early brain injury in subarachnoid hemorrhage. Transl Stroke Res. 2022;13:112–31.
25. Mu Q, Yao K, Syeda MZ, Wan J, Cheng Q, You Z, Sun R, Zhang Y, Zhang H, Lu Y, et al. Neutrophil targeting platform reduces neutrophil extracellular traps for improved traumatic brain injury and stroke theranostics. Adv Sci. 2024;11: e2308719.
26. Griton M, Dhaya I, Nicolas R, Raffard G, Periot O, Hiba B, Konsman JP. Experimental sepsis-associated encephalopathy is accompanied by altered cerebral blood perfusion and water diffusion and related to changes in cyclooxygenase-2 expression and glial cell morphology but not to blood-brain barrier breakdown. Brain Behav Immun. 2020;83:200–13.
27. Fu Q, Wu J, Zhou XY, Ji MH, Mao QH, Li Q, Zong MM, Zhou ZQ, Yang JJ. NLRP3/caspase-1 pathway-induced pyroptosis mediated cognitive deficits in a mouse model of sepsis-associated encephalopathy. Inflammation. 2019;42:306–18.
28. Yue J, Tan Y, Huan R, Guo J, Yang S, Deng M, Xiong Y, Han G, Liu L, Liu J, et al. Mast cell activation mediates blood-brain barrier impairment and cognitive dysfunction in septic mice in a histamine-dependent pathway. Front Immunol. 2023;14:1090288.
29. Wang Y, Sha H, Zhou L, Chen Y, Zhou Q, Dong H, Qian Y. The mast cell is an early activator of lipopolysaccharide-induced neuroinflammation and blood–brain barrier dysfunction in the hippocampus. Mediators Inflamm. 2020;2020:8098439.
30. Zhao P, Li Y, Xu X, Yang H, Li X, Fu S, Guo Z, Zhang J, Li H, Tian J. Neutrophil extracellular traps mediate cardiomyocyte ferroptosis via the Hippo-Yap pathway to exacerbate doxorubicin-induced cardiotoxicity. Cell Mol Life Sci. 2024;81:122.
31. Jin J, Wang F, Tian J, Zhao X, Dong J, Wang N, Liu Z, Zhao H, Li W, Mang G, et al. Neutrophil extracellular traps contribute to coagulopathy after traumatic brain injury. JCI Insight. 2023;8: e141110.
32. Ahishali B, Kaya M. Evaluation of blood–brain barrier integrity using vascular permeability markers: evans blue, sodium fluorescein, albumin-alexa fluor conjugates, and horseradish peroxidase. Methods Mol Biol. 2021;2367:87–103.
33. Shen Y, Zhang Y, Du J, Jiang B, Shan T, Li H, Bao H, Si Y. CXCR5 downregulation alleviates cognitive dysfunction in a mouse model of sepsis-associated encephalopathy: potential role of microglial autophagy and the p38MAPK/NF-κB/STAT3 signaling pathway. J Neuroinflamm. 2021;18:246.
34. Nishibori M, Wang D, Ousaka D, Wake H. High mobility group box-1 and blood–brain barrier disruption. Cells. 2020;9:2650.
35. Kadry H, Noorani B, Cucullo L. A blood-brain barrier overview on structure, function, impairment, and biomarkers of integrity. Fluids Barriers CNS. 2020;17:69.
36. Bronstein JM, Micevych PE, Chen K. Oligodendrocyte-specific protein (OSP) is a major component of CNS myelin. J Neurosci Res. 1997;50:713–20.
37. Maheras KJ, Peppi M, Ghoddoussi F, Galloway MP, Perrine SA, Gow A. Absence of claudin 11 in CNS myelin perturbs behavior and neurotransmitter levels in mice. Sci Rep. 2018;8:3798.
38. Reinhold AK, Rittner HL. Barrier function in the peripheral and central nervous system-a review. Pflugers Arch. 2017;469:123–34.
39. Tietz S, Engelhardt B. Brain barriers: crosstalk between complex tight junctions and adherens junctions. J Cell Biol. 2015;209:493–506.
40. Matter K, Balda MS. Signalling to and from tight junctions. Nat Rev Mol Cell Biol. 2003;4:225–36.
41. Pal I, Rajesh Y, Banik P, Dey G, Dey KK, Bharti R, Naskar D, Chakraborty S, Ghosh SK, Das SK, et al. Prevention of epithelial to mesenchymal transition in colorectal carcinoma by regulation of the E-cadherin-β-catenin-vinculin axis. Cancer Lett. 2019;452:254–63.
42. Torres-Iberico R, Condori-Fernández Y, Apagüeño-Ruiz C, Andia-Ticona M, Pomar-Morante R. Kindler syndrome: a multidisciplinary management approach. Actas Dermosifiliogr. 2020;111:775–80.
43. Huang CY, Wei PL, Batzorig U, Makondi PT, Lee CC, Chang YJ. Identification of moesin (MSN) as a potential therapeutic target for colorectal cancer via the β-catenin-RUNX2 Axis. Int J Mol Sci. 2023;24:10951.
44. Peng X, Cuff LE, Lawton CD, DeMali KA. Vinculin regulates cell-surface E-cadherin expression by binding to beta-catenin. J Cell Sci. 2010;123:567–77.
45. Harris ES, Nelson WJ. VE-cadherin: at the front, center, and sides of endothelial cell organization and function. Curr Opin Cell Biol. 2010;22:651–8.
46. Yue J, Zhang J, Huan R, Zeng Y, Tan Y, Cheng Y. Dishevelled-associated antagonist of β-catenin homolog 3 (DACT3) suppresses glioma progression though Notch1 signaling pathway in β-catenin-dependent manner. Heliyon. 2024;10: e23511.
47. Wang R, Zhu Y, Liu Z, Chang L, Bai X, Kang L, Cao Y, Yang X, Yu H, Shi MJ, et al. Neutrophil extracellular traps promote tPA-induced brain hemorrhage via cGAS in mice with stroke. Blood. 2021;138:91–103.
48. Denorme F, Portier I, Rustad JL, Cody MJ, de Araujo CV, Hoki C, Alexander MD, Grandhi R, Dyer MR, Neal MD, et al. Neutrophil extracellular traps regulate ischemic stroke brain injury. J Clin Invest. 2022;132: e154225.
49. Shi G, Liu L, Cao Y, Ma G, Zhu Y, Xu J, Zhang X, Li T, Mi L, Jia H, et al. Inhibition of neutrophil extracellular trap formation ameliorates neuroinflammation and neuronal apoptosis via STING-dependent IRE1α/ASK1/JNK signaling pathway in mice with traumatic brain injury. J Neuroinflamm. 2023;20:222.
50. Abrams ST, Morton B, Alhamdi Y, Alsabani M, Lane S, Welters ID, Wang G, Toh CH. A novel assay for neutrophil extracellular trap formation independently predicts disseminated intravascular coagulation and mortality in critically ill patients. Am J Respir Crit Care Med. 2019;200:869–80.
51. Maruchi Y, Tsuda M, Mori H, Takenaka N, Gocho T, Huq MA, Takeyama N. Plasma myeloperoxidase-conjugated DNA level predicts outcomes and organ dysfunction in patients with septic shock. Crit Care. 2018;22:176.
52. McDonald B, Davis RP, Kim SJ, Tse M, Esmon CT, Kolaczkowska E, Jenne CN. Platelets and neutrophil extracellular traps collaborate to promote intravascular coagulation during sepsis in mice. Blood. 2017;129:1357–67.
53. Alsabani M, Abrams ST, Cheng Z, Morton B, Lane S, Alosaimi S, Yu W, Wang G, Toh CH. Reduction of NETosis by targeting CXCR1/2 reduces thrombosis, lung injury, and mortality in experimental human and murine sepsis. Br J Anaesth. 2022;128:283–93.
54. Huang J, Hong W, Wan M, Zheng L. Molecular mechanisms and therapeutic target of NETosis in diseases. MedComm. 2020;2022(3): e162.
55. Zhao Y, Gan L, Ren L, Lin Y, Ma C, Lin X. Factors influencing the blood-brain barrier permeability. Brain Res. 2022;1788:147937.
56. Riedhammer KM, Stockler S, Ploski R, Wenzel M, Adis-Dutschmann B, Ahting U, Alhaddad B, Blaschek A, Haack TB, Kopajtich R, et al. De novo stop-loss variants in CLDN11 cause hypomyelinating leukodystrophy. Brain. 2021;144:411–9.
57. Devaux J, Gow A. Tight junctions potentiate the insulative properties of small CNS myelinated axons. J Cell Biol. 2008;183:909–21.
58. Lan S, Zheng X, Hu P, Xing X, Ke K, Wang F, Cheng N, Zhuang Q, Liu X, Liu J, et al. Moesin facilitates metastasis of hepatocellular carcinoma cells by improving invadopodia formation and activating β-catenin/MMP9 axis. Biochem Biophys Res Commun. 2020;524:861–8.
59. Wang Q, Lu X, Wang J, Yang Z, Hoffman RM, Wu X. Moesin up-regulation is associated with enhanced tumor progression imaged non-invasively in an orthotopic mouse model of human glioblastoma. Anticancer Res. 2018;38:3267–72.
60. Wang W, Kansakar U, Markovic V, Sossey-Alaoui K. Role of Kindlin-2 in cancer progression and metastasis. Ann Transl Med. 2020;8:901.
61. Liu CC, Cai DL, Sun F, Wu ZH, Yue B, Zhao SL, Wu XS, Zhang M, Zhu XW, Peng ZH, et al. FERMT1 mediates epithelial-mesenchymal transition to promote colon cancer metastasis via modulation of β-catenin transcriptional activity. Oncogene. 2017;36:1779–92.
62. Leerberg JM, Yap AS. Vinculin, cadherin mechanotransduction and homeostasis of cell-cell junctions. Protoplasma. 2013;250:817–29.
63. Zhong W, Yang W, Qin Y, Gu W, Xue Y, Tang Y, Xu H, Wang H, Zhang C, Wang C, et al. 6-Gingerol stabilized the p-VEGFR2/VE-cadherin/β-catenin/actin complex promotes microvessel normalization and suppresses tumor progression. J Exp Clin Cancer Res. 2019;38:285.

64. Guo M, Breslin JW, Wu MH, Gottardi CJ, Yuan SY. VE-cadherin and beta-catenin binding dynamics during histamine-induced endothelial hyperpermeability. Am J Physiol Cell Physiol. 2008;294:C977-984.
65. Hermann DM, ElAli A. The abluminal endothelial membrane in neurovascular remodeling in health and disease. Sci Signal. 2012;5: re4.
66. Wang L, Geng J, Qu M, Yuan F, Wang Y, Pan J, Li Y, Ma Y, Zhou P, Zhang Z, et al. Oligodendrocyte precursor cells transplantation protects blood-brain barrier in a mouse model of brain ischemia via Wnt/β-catenin signaling. Cell Death Dis. 2020;11:9.
67. Hübner K, Cabochette P, Diéguez-Hurtado R, Wiesner C, Wakayama Y, Grassme KS, Hubert M, Guenther S, Belting HG, Affolter M, et al. Wnt/β-catenin signaling regulates VE-cadherin-mediated anastomosis of brain capillaries by counteracting S1pr1 signaling. Nat Commun. 2018;9:4860.
68. Liu X, Su P, Meng S, Aschner M, Cao Y, Luo W, Zheng G, Liu M. Role of matrix metalloproteinase-2/9 (MMP2/9) in lead-induced changes in an in vitro blood-brain barrier model. Int J Biol Sci. 2017;13:1351–60.
69. Shi T, Yue S, Xie C, Li X, Yang D, Hu L, Zhong Y, Zhang Y, Liu W. MMP-2-mediated Scube2 degradation promotes blood-brain barrier disruption by blocking the interaction between astrocytes and endothelial cells via inhibiting Sonic hedgehog pathway during early cerebral ischemia. J Neurochem. 2023. https://doi.org/10.1111/jnc.16021.
70. Daneman R, Agalliu D, Zhou L, Kuhnert F, Kuo CJ, Barres BA. Wnt/beta-catenin signaling is required for CNS, but not non-CNS, angiogenesis. Proc Natl Acad Sci USA. 2009;106:641–6.
71. Liebner S, Corada M, Bangsow T, Babbage J, Taddei A, Czupalla CJ, Reis M, Felici A, Wolburg H, Fruttiger M, et al. Wnt/beta-catenin signaling controls development of the blood-brain barrier. J Cell Biol. 2008;183:409–17.
72. Song S, Huang H, Guan X, Fiesler V, Bhuiyan MIH, Liu R, Jalali S, Hasan MN, Tai AK, Chattopadhyay A, et al. Activation of endothelial Wnt/β-catenin signaling by protective astrocytes repairs BBB damage in ischemic stroke. Prog Neurobiol. 2021;199:101963.
73. Stenman JM, Rajagopal J, Carroll TJ, Ishibashi M, McMahon J, McMahon AP. Canonical Wnt signaling regulates organ-specific assembly and differentiation of CNS vasculature. Science. 2008;322:1247–50.
74. Chang J, Mancuso MR, Maier C, Liang X, Yuki K, Yang L, Kwong JW, Wang J, Rao V, Vallon M, et al. Gpr124 is essential for blood–brain barrier integrity in central nervous system disease. Nat Med. 2017;23:450–60.
75. Corada M, Orsenigo F, Bhat GP, Conze LL, Breviario F, Cunha SI, Claesson-Welsh L, Beznoussenko GV, Mironov AA, Bacigaluppi M, et al. Fine-tuning of Sox17 and canonical Wnt coordinates the permeability properties of the blood-brain barrier. Circ Res. 2019;124:511–25.
76. Wang W, Li M, Wang Y, Wang Z, Zhang W, Guan F, Chen Q, Wang J. GSK-3β as a target for protection against transient cerebral ischemia. Int J Med Sci. 2017;14:333–9.
77. Valenta T, Hausmann G, Basler K. The many faces and functions of β-catenin. EMBO J. 2012;31:2714–36.
78. Lengfeld JE, Lutz SE, Smith JR, Diaconu C, Scott C, Kofman SB, Choi C, Walsh CM, Raine CS, Agalliu I, et al. Endothelial Wnt/β-catenin signaling reduces immune cell infiltration in multiple sclerosis. Proc Natl Acad Sci USA. 2017;114:E1168-e1177.
79. Gao K, Shao W, Wei T, Yan Z, Li N, Lv C. Wnt-3a improves functional recovery after spinal cord injury by regulating the inflammatory and apoptotic response in rats via wnt/β-catenin signaling pathway. Brain Res. 2024;1822:148637.
80. Lilien J, Balsamo J. The regulation of cadherin-mediated adhesion by tyrosine phosphorylation/dephosphorylation of beta-catenin. Curr Opin Cell Biol. 2005;17:459–65.
81. Zeng Y, Zhang J, Yue J, Han G, Liu W, Liu L, Lin X, Zha Y, Liu J, Tan Y. The role of DACT family members in tumorigenesis and tumor progression. Int J Biol Sci. 2022;18:4532–44.

Publisher's Note